Host-directed therapy for the treatment of tuberculosis: rewiring the host to recover control

Heemskerk, M.T.

CHAPTER 6

Functional Inhibition of Host Histone Deacetylases (HDACs) Enhances in vitro and in vivo Anti-mycobacterial Activity in Human Macrophages and in Zebrafish

J.D. Moreira[1,2], B.E.V. Koch[3], S. van Veen[1], K.V. Walburg[1], F. Vrieling[1], T.M. Pinto Dabés Guimarães[2], A.H. Meijer[3], H.P. Spaink[3], T.H.M. Ottenhoff[1], M.C. Haks[1]*, and M.T. Heemskerk[1]*

[1] Department of Infectious Diseases, Leiden University Medical Center, Leiden, The Netherlands.
[2] Department of Clinical and Toxicological Analysis, Faculty of Pharmacy, Federal University of Minas Gerais, Belo Horizonte, Minas Gerais, Brazil.
[3] Institute of Biology Leiden, Leiden University, Leiden, The Netherlands.
* These authors have contributed equally to this work.

Frontiers in Immunology (2020)
DOI: 10.3389/fimmu.2020.00036

Abstract

The rapid and persistent increase of drug-resistant *Mycobacterium tuberculosis* (*Mtb*) infections poses increasing global problems in combatting tuberculosis (TB), prompting for the development of alternative strategies including host-directed therapy (HDT). Since *Mtb* is an intracellular pathogen with a remarkable ability to manipulate host intracellular signalling pathways to escape from host defence, pharmacological reprogramming of the immune system represents a novel, potentially powerful therapeutic strategy that should be effective also against drug-resistant *Mtb*. Here, we found that host-pathogen interactions in *Mtb*-infected primary human macrophages affected host epigenetic features by modifying histone deacetylase (HDAC) transcriptomic levels. In addition, broad spectrum inhibition of histone deacetylases enhanced the antimicrobial response of both pro-inflammatory macrophages (Mϕ1) and anti-inflammatory macrophages (Mϕ2), while selective inhibition of class IIa HDACs mainly decreased bacterial outgrowth in Mϕ2. Moreover, chemical inhibition of HDAC activity during differentiation polarized macrophages into a more bactericidal phenotype with a concomitant decrease in the secretion levels of inflammatory cytokines. Importantly, *in vivo* chemical inhibition of HDAC activity in *Mycobacterium marinum*-infected zebrafish embryos, a well characterized animal model for tuberculosis, significantly reduced mycobacterial burden, validating our *in vitro* findings in primary human macrophages. Collectively, these data identify HDACs as druggable host targets for HDT against intracellular *Mtb*.

Introduction

Tuberculosis (TB) is a health threat of global dimensions, and is caused by the highly successful human pathogen *Mycobacterium tuberculosis* (*Mtb*). Remarkably, *Mtb* is capable of establishing intracellular infection even in the presence of strong innate and adaptive host immunity. One fourth of the global human population is estimated to be latently infected with *Mtb*. These individuals have a 5-10% lifetime risk of developing TB reactivation disease, resulting in 10 million people falling ill with TB and over 1.5 million deaths each year [6]. In HIV-infected or otherwise immunocompromised patients the risk of TB reactivation is significantly increased.

Current interventions (antibiotics, BCG vaccination) fail to reduce TB incidence sufficiently. Together with the rising frequency of multi-, extensively-, and even totally drug-resistant (MDR/XDR/TDR) *Mtb* strains, and the fact that many druggable targets in pathogens are already inhibited by current antibiotics [441], it is crucial to develop new and much more effective strategies that act by mechanisms different from those already targeted by current interventions. Since *Mtb* has a remarkable ability to manipulate intracellular signalling pathways which promote its escape from host defence in human cells, host-directed therapies (HDT) would represent a therapeutic strategy that would be effective also against currently untreatable strains since these compounds act on host and not on pathogen molecules.

TB most commonly presents as a pulmonary disease following inhalation of *Mtb*-containing droplets in the lung. Modulation of host signalling pathways by *Mtb* in infected alveolar macrophages arrests phagosome maturation to create a niche for its intracellular survival [442, 443]. In addition, activation of alveolar macrophages results in transcriptional changes that regulate innate and adaptive immune responses such as production of chemokines and pro- and anti-inflammatory cytokines [444]. Epigenetic regulators play a crucial role in regulating the transcriptional response to microorganisms by chromatin remodelling [445, 446]. Acetylation of histone proteins is one of the main mechanisms to control DNA accessibility and thereby gene expression [447]. Histone acetyltransferases (HATs) acetylate lysine residues in histone tails resulting in a more relaxed chromatin structure which is associated with transcriptional activation. In contrast, histone-deacetylases (HDACs) counteract the activity of HATs by removing acetyl groups from highly conserved lysine residues resulting in more condensed chromatin structure which is associated with transcriptional repression by limiting the accessibility to the transcriptional machinery. HDACs are divided into four classes: Class I (HDAC1, 2, 3, and 8), class II (class IIa HDAC4, 5, 7 and 9; class IIb HDAC6 and 10), class III (SIRT1-7) and class IV (HDAC11) based on their function, co-factor dependency and structural homology to yeast

HDACs [448]. Class I, II, and IV enzymes belong to the family of 'classical' HDACs and have a zinc-dependent active site, whereas class III proteins are NAD^+-dependent and considered a family of 'non-classical' HDACs.

HDACs are important players in the differentiation of macrophages and their role in immunity. HDAC3 has been shown to be vital in the development of anti-inflammatory macrophages (Mϕ2) by repressing alternative macrophage activation [449] whereas pro-inflammatory macrophages (Mϕ1) are impacted by several HDACs, such as HDAC4, 5, 6 and 7, which strongly regulate the expression of pro-inflammatory genes upon stimulation with *e.g.* lipopolysaccharide (LPS) [450-452]. Granuloma formation is driven by macrophages and the resulting outcome of infection, i.e. bacterial control or bacterial dissemination, relies on macrophage type and polarization [96, 453]. It is therefore not surprising that several pathogens, including *Mtb* have been implicated in evading the immune system by modulating histone acetylation via altering HDAC expression levels [450, 454-457].

In the present study, we investigated the expression kinetics of different classes of HDAC transcripts in response to *Mtb* infection in primary human macrophages and found expression levels of a diverse set of HDAC genes to be affected by *Mtb*. We next investigated the impact of HDAC inhibition on infection in human macrophages *in vitro*. A pan-HDAC inhibitor as well as several selective class IIa inhibitors significantly reduced outgrowth of intracellular *Mtb* in macrophages. Importantly these results were validated in an *in vivo* model of tuberculosis, the *Mycobacterium marinum* zebrafish embryo infection model [57, 458, 459]. Collectively these results establish the potential of HDAC inhibitors as novel host-directed therapeutics for TB.

Materials and Methods

Reagents

H-89 dihydrochloride (PKA/PKB/AKT1 kinase inhibitor), 3-aminobenzoic acid ethyl ester (tricaine) and rifampicin were purchased from Sigma-Aldrich, Zwijndrecht, The Netherlands. H-89 analogue 97i was synthesized by the Leiden Academic Centre for Drug Research, Division of Medicinal Chemistry, Leiden University, Leiden, The Netherlands. Pan-HDAC inhibitor Trichostatin A (TSA) and class IIa HDAC inhibitors TMP195 and TMP269 were purchased from Selleckchem, Munich, Germany. Hygromycin B was acquired from Life Technologies-Invitrogen, Bleiswijk, The Netherlands. Recombinant human IFN-γ protein was acquired from R&D Systems, Wiesbaden, Germany.

Cell culture

Peripheral blood mononuclear cells (PBMCs) were isolated from buffy coats obtained from healthy donors after written informed consent (Sanquin Blood Bank, Amsterdam, The Netherlands). Monocytes were isolated through density gradient centrifugation over Ficoll-Paque followed by CD14 MACS sorting (Miltenyi Biotec, Bergisch Gladsbach, Germany) and differentiated for 6 days into pro-inflammatory (Mϕ1) or anti-inflammatory (Mϕ2) macrophages with 5 ng/ml of granulocyte-macrophage colony-stimulating factor (GM-CSF; Life Technologies-Invitrogen) or 50 ng/ml macrophage colony-stimulating factor (M-CSF; R&D Systems, Abingdon, UK), respectively, as previously reported [311]. Cells were cultured at 37°C/5% CO_2 in Gibco Roswell Park Memorial Institute (RPMI) 1640 medium (Life Technologies-Invitrogen) supplemented with 10% FBS and 2 mM L-alanyl-L-glutamine (GlutaMAX) (PAA, Linz, Austria), 100 U/ml penicillin and 100 µg/ml streptomycin (Life Technologies-Invitrogen). Macrophage differentiation and activation was checked by quantifying IL-12p40 and IL-10 secretion (for Mϕ1 and Mϕ2, respectively) using ELISA in the presence or absence of 24 hour stimulation with 100 ng/ml of lipopolysaccharide (LPS) (InvivoGen, San Diego, United States).

Mtb infection of macrophages

Mtb (DsRed-expressing H37Rv [243]) was cultured in Difco Middlebrook 7H9 broth (Becton Dickinson, Breda, The Netherlands) supplemented with 10% ADC (Becton Dickinson) and 0.05% Tween 80 (Sigma-Aldrich). One day before infection, *Mtb* cultures were diluted to a density corresponding with early log-phase growth (OD_{600} of 0.25). The following day, bacterial suspensions (or 7H9 for mock infections) were diluted in cell culture medium without antibiotics to reach a multiplicity of infection (MOI) of 10. MOI of the inoculum was verified by a standard colony-forming unit (CFU) assay. Cells seeded in 96-well flat-bottom plates at a density of 30,000 cells/well in

appropriate cell culture medium without antibiotics 1 day prior to infection, were inoculated with 100 µl of the bacterial suspension, centrifuged for 3 min at 800 rpm, and incubated at 37°C/5% CO_2 for 60 min. Bacteria were then washed away with cell culture medium containing 30 µg/ml gentamicin sulfate (Lonza BioWhittaker, Basel, Switzerland), incubated for 10 min at 37°C/5% CO_2, followed by replacement with medium containing 5 µg/ml gentamicin sulfate and, if indicated, chemical compounds until readout by flow cytometry, Luminex or CFU.

Chemical compound treatment

During differentiation, monocytes were treated for 6 days with 300 nM TMP195, 300 nM TMP269, 30 nM TSA or DMSO at equal v/v [460]. The TMP195 and TMP269 concentration of 300 nM was based on the results reported by Guerriero, Sotayo [461] in a similar model of monocyte differentiation and was not toxic. TSA, however, was used at a concentration of 30 nM which was safe for 6 days while higher concentrations showed toxicity. Alternatively, *Mtb*-infected Mϕ1 and Mϕ2 were treated for 48h with 10 µM TMP195, TMP269, H-89 and 97i, 100 nM TSA or DMSO at equal v/v in medium containing 5 µg/ml gentamicin sulfate. Prior to these experiments, we had performed pilot experiments to exclude cellular toxicity on primary macrophages. We found no toxicity for both TMP195 as well as TMP269 at concentrations of 10 µM, which constitutes a standard concentration in initial drug screening, confirming results from Lobera, Madauss [460]. Trichostatin A, however, was found to be highly toxic at 10 µM and was therefore evaluated at lower concentrations. A concentration of 0.1 µM was found to be non-toxic in our primary human macrophage model, agreeing well with previously published results [462].

Zebrafish handling, compound treatment and *Mycobacterium marinum* infection

Zebrafish were handled in compliance with animal welfare regulations and maintained according to standard protocols (http://zfin.org). Fertilized embryos were maintained at 28°C and kept in egg water (60 µg/ml Instant Ocean Sea Salt, Sera, Heinsberg Germany). Zebrafish embryos starting the 20 somite stage were exposed for the following 24 hours to 10 µM TMP195, 30 nM TSA or DMSO at equal v/v in egg water at 28°C. *Mycobacterium marinum* (*Mmar*) M-strain carrying a plasmid encoding the Wasabi fluorescent protein [393] was cultured in 7H9 medium with 10% BBL ADC enrichment medium, BD, Franklin Lakes, United States) and 50 µg/ml Hygromycin at 28°C, to an optical density OD_{600} of approximately 1. For the duration of bacterial injections, zebrafish larvae were kept under anesthesia in egg water containing 0.02% buffered 3-aminobenzoic acid ethyl ester (tricaine) and infections were performed by microinjection of 250-300 CFU into the Duct of Cuvier at approximately 43 hours post

fertilization (hpf), 24 hours post treatment, as previously described [394]. At three days post infection (dpi), the infection was quantified by fluorescent pixel determination [395]. Infected embryos were anaesthetized using 0.02% tricaine in egg water and imaged using a Leica MZ16FA Fluorescence Stereo Microscope (Leica Microsystems, Wetzlar, Germany) equipped with a DFC420C color camera (Leica Microsystems, Wetzlar, Germany).

Colony-forming unit (CFU) assay

CFU spot assays have been described elsewhere [463]. Briefly, cells were lysed in H_2O containing 0.05% SDS. Cell lysates were serially diluted in multiple steps of 5-fold dilutions in 7H9 broth and 10 µl droplets were spotted onto square Middlebrook 7H10 agar plates and incubated for 12-14 days at 37°C. Bacterial colonies were enumerated using a microscope with a magnification of 2.5 times to enhance early detection of bacterial growth.

Mtb growth assay

A volume of 100 µl of *Mtb* culture (OD_{600} of 0.2) in 7H9 broth was plated in a flat-bottom 96-well plate containing 100 µl of 7H9 broth with TMP195, TMP269, TSA or Rifampicin as a positive control or DMSO at equal v/v at indicated concentrations. Growth was evaluated at 37°C for 13 days and absorbance was measured by optical density at 550 nm on a Mithras LB 940 plate reader (Berthold Technologies, Bad Wildbad, Germany).

Flow cytometry

Single cell suspensions were incubated for 5 min with 5% human serum (Sanquin Blood Bank) in PBS to block non-specific Fc-receptor binding, washed in PBS/0.1% BSA (Merck, Darmstadt, Germany) and stained with monoclonal antibodies against cell surface markers CD11b-PE, CD1a-BV605, CD80-FITC, CD86-AF700 (all BD BioSciences, Vianen, The Netherlands), CD14-FITC and CD163-AF647 (BioLegend, San Diego, CA, USA) for 30 min at 4°C. Cells were washed twice in PBS/0.1% BSA and acquisition was performed using a BD FACSLyric™ Flow Cytometer (BD Biosciences). Data was analyzed using FlowJo v10 software.

Cell viability assay

Cells seeded at a density of 30,000 cells/well in 96-well flat-bottom plates were stained in 50 µl cell culture medium without phenol red containing propidium iodide (PI) (1:500, Sigma-Aldrich) and Hoechst (1:100, Sigma-Aldrich). After incubation for 5 min at room temperature (RT), 3 images per well were recorded using a Leica AF6000 LC fluorescence microscope combined with a 20x dry objective. Cell viability was calculated by quantifying the number of dead cells (PI positive) versus total cell numbers (Hoechst positive) using ImageJ software.

Microscopy

Bright field image acquisition was performed using an Olympus IX51 Inverted Microscope combined with Olympus cellSens software.

Cytokine and chemokine multiplex beads assay

Culture supernatants were collected 24h post-infection and filter-sterilized by centrifugation in 96-well filter plates containing a 0.2 µm PVDF membrane (Corning, Amsterdam, The Netherlands). Forty-one analytes were quantified using the Milliplex Human Cytokine/chemokine magnetic bead premixed 41-plex kit (Millipore Billerica, MA, USA) according to the manufacturer's instructions. Analyses were performed on a Bio-Plex 100 with Bio-Plex Manager™ software v6.1 (Biorad, Veenendaal, The Netherlands).

The following analytes were measured: sCD40L, EGF, FGF-2, Flt3 ligand, Fractalkine (CX3CL1), G-CSF, GM-CSF, GRO (CXCL1), IFN-γ, IFN-α2, IL-1α, IL-1β, IL-1ra, IL-2, IL-3, IL-4, IL-5, IL-6, IL-7, IL-8 (CXCL8), IL-9, IL-10, IL-12p40, IL-12p70, IL-13, IL-15, IL-17a, IP-10 (CXCL10), MCP-1 (CCL2), MCP-3 (CCL7), MDC (CCL22), MIP-1α (CCL3), MIP-1β (CCL4), PDGF-AB/BB, RANTES (CCL5), TGF-α, TNF-α, TNF-β, VEGF, Eotaxin (CCL11) and PDGF-AA.

Phagocytosis assay

Cells were pulsed with Fluoresbrite® YG Carboxylate Microspheres P beads (Polysciences, Warrington, PA, USA) in a ratio of 10 beads to 1 cell for 90 min at 37°C/5% CO_2. Cells were subsequently washed with PBS and harvested by adding Trypsin-EDTA 0.5% (ThermoFisher Scientific, Waltham, MA, USA). Cells were centrifuged and resuspended in 100 µl Trypan Blue (1:1) in PBS/0.1% BSA (Merck) to quench fluorescence of extracellular beads. Internalized beads were quantified by flow cytometry on a BD FACSLyric™. Data analysis was performed using FlowJo v10 software.

Total RNA isolation and cDNA synthesis

Total RNA isolation was performed using TRIzol Reagent (Life Technologies-Invitrogen) according to the manufacturer's instructions and RNA yield was quantified using a DeNovix DS-11 Spectrophotometer (ThermoFisher Scientific). Total RNA (0.5 µg) was reverse transcribed using SuperScript IV Reverse Transcriptase (Life Technologies-Invitrogen). Briefly, RNA samples were first incubated at 65°C for 5 min in the presence of 0.5 mM dNTPs and 2.5 µM oligo$(dT)_{20}$ (Life Technologies-Invitrogen). Subsequently, cDNA synthesis was initiated by adding a master mix containing 1x first strand buffer, 5 mM DTT, 40 U RNaseOUT (ThermoFisher Scientific) and 200 U SuperScript IV and

incubating at 50-55°C for 10 min followed by inactivation of the reverse transcriptase at 80°C for 10 min.

TaqMan qPCR

Multiplex quantitative polymerase chain reaction (qPCR) was carried out using a QuantStudio 6 Flex Real-Time PCR System (ThermoFisher Scientific). qPCR reactions were performed in a final volume of 25 µl containing 1x TaqMan Universal PCR Master Mix, No AmpErase UNG, 1x HDAC(1-11)-FAM TaqMan primers (ThermoFisher Scientific), 0.5x GAPDH-VIC TaqMan primers (ThermoFisher Scientific), and 20 ng cDNA. Thermal cycling conditions were 1 cycle of 2 min/50°C and 10 min/95°C, followed by 60 cycles of 15s/95°C and 1 min/60°C. Relative expression levels were calculated by applying the formula $((2^{-\Delta CT(\text{Target gene})})/(2^{-\Delta CT(GAPDH)}))$ The threshold cycle (Ct) values of HDAC transcripts were normalized to GAPDH by the $2^{-\Delta\Delta CT}$ algorithm method [313]. The following TaqMan® Gene Expression Assays were used: GAPDH-VIC (Hs02758991_g1), HDAC1-FAM (Hs00606262_g1), HDAC2-FAM (Hs00231032_m1), HDAC3-FAM (Hs00187320_m1), HDAC4-FAM (Hs01041638_m1), HDAC5-FAM (Hs00608351_m1), HDAC6-FAM (Hs00997427_m1), HDAC7-FAM (Hs00248789_m1), HDAC8-FAM (Hs00954353_g1), HDAC9-FAM (Hs01081558_m1), HDAC10-FAM (Hs00368899_m1), HDAC11-FAM (Hs00978038_m1), TNF-FAM (Hs00174128_m1), IL6-FAM (Hs00174131_m1), CSF3-FAM (Hs00738432_g1), IFNG-FAM (Hs00989291_m1), CCL2-FAM (Hs00234140_m1), CCL3-FAM (Hs00234142_m1), CCL4-FAM (Hs99999148_m1) and CXCL8-FAM (Hs00174103_m1). TNF, IL6, CSF3 and IFNG could not be detected within a cycle threshold (Ct) of 45.

Data analysis

Normal distribution of data sets was evaluated using the Shapiro-Wilk normality test. Paired sample t-test analysis was employed when comparing two experimental conditions. One-way ANOVA and repeated measure (RM) one-way ANOVA with Dunnett's multiple test correction were applied when assessing differences between 3 or more groups of unpaired and paired samples, respectively. Zebrafish embryo infection data was tested for significance using a Kruskal-Wallis test followed by Dunnett's multiple test correction. All analyses were performed using GraphPad Prism 8.

For multilevel partial least squares-discriminant analysis (PLS-DA) [464], the R package mixOmics (version 6.3.2) was used [465]. Model validity was assessed by determining model quality characteristics for explained variance (R^2X, R^2Y) and predictive ability (Q^2_{cum}) after leave-one-out cross validation (LOOCV). Variable Importance in Projection (VIP) scores of the first x-variate, representing the contribution of each variable to the model, were extracted from each PLS-DA analysis

and values equal or greater than 1 were considered relevant. Only analytes that changed in at least 3 out of 4 donors with a minimal median $\log_2$ fold change (FC) of 0.5 were included in the analyses. The associations of analytes with treatment response are reflected by Kendall correlation coefficients. For calculation of the Kendall rank correlation coefficient tau-b, the R package Kendall (version 2.2) was used [466].

Fluorescent images of infected zebrafish embryos in Tiff file format were processed and quantified using the Fiji distribution of ImageJ [312]. For the processing steps, involving thresholding and quantification of positive pixels, an ImageJ macro was developed: run("8-bit"); setAutoThreshold("Triangle dark"); setThreshold(4, 255); run("Convert to Mask"); run("Measure"); close().

Results

Regulation of HDAC transcriptomic profiles in response to *Mtb* infection.

To explore whether intracellular survival of *Mtb* is controlled by host epigenetic features, we investigated whether *Mtb*-H37Rv (*Mtb*) infection could impact histone acetylation in primary human pro-inflammatory (Mϕ1) and anti-inflammatory (Mϕ2) macrophages (the main target cell of *Mtb*), representing opposing ends of the macrophage differentiation spectrum. Expression kinetics of all eleven canonical HDAC transcripts were determined in triplicate by qRT-PCR before (baseline) and 4 and 24h following infection with *Mtb* (**Figure 1**). Differential regulation of HDAC transcript levels upon *Mtb* infection was more pronounced in Mϕ2 than Mϕ1. HDAC1 was substantially upregulated 24h post-infection in both Mϕ1 and Mϕ2. In contrast, expression levels of HDAC3, 5, 7, 10 and 11 were significantly repressed in Mϕ2 whereas in Mϕ1 this was only observed for HDAC5. Interestingly, expression levels of 4 out of 5 HDACs that were significantly suppressed in Mϕ2 following infection with *Mtb*, exhibited significantly higher transcript levels in Mϕ2 compared to Mϕ1 at baseline. (**Supplementary Figure 1A**). Since HDACs are considered molecular switches regulating a plethora of processes including balancing pro-versus anti-inflammatory responses (**Supplementary Table 1**), distinct baseline expression levels of HDAC family members might explain differences in inflammatory cytokine profiles between activated Mϕ1 and Mϕ2 [311]. Using a published RNA-sequencing dataset of *Mtb*-infected Mϕ2, we were able to independently validate our findings (markedly enhanced expression levels of HDAC1 and significantly reduced transcript levels of HDAC3, 5, 10 and 11 upon infection with *Mtb*-H37Rv, heat-killed *Mtb*-H37Rv and Bacillus Calmette-Guérin (BCG)) for anti-inflammatory macrophages (**Supplementary Figure 1B**) [467].

Interestingly, this lower expression levels were not seen at early timepoints after infection with *Mtb*-GC1237, a virulent Beijing strain, implying that this could be advantageous to the pathogen. This suggests that lowering these specific HDAC expression levels might be beneficial to the host. Together, these data suggest that host-pathogen interactions in *Mtb*-infected macrophages affect host epigenetic features by modifying histone acetylation through regulating HDAC expression levels. Therefore, targeting HDACs with small molecules could potentially regulate outgrowth of intracellular infections with *Mtb*.

Chemical inhibition of HDACs markedly reduces intracellular survival of *Mtb*.

To investigate whether histone acetylation/deacetylation controls *Mtb* infection, *Mtb*-infected Mϕ1 and Mϕ2 were treated with selective class IIa HDAC inhibitors (TMP195 and TMP269 [460]) or the pan-HDAC inhibitor Trichostatin A (TSA) (**Figure 2A**). Given the nature and mechanisms of action of the HDAC targets (which enzymatically control epigenetic state), we hypothesized that a higher end dose of inhibitors was needed to be able to measure a phenotype in *Mtb*-infected cells [468]. Pan-HDAC inhibition by TSA significantly reduced bacterial load in both Mϕ1 and Mϕ while selective inhibition of class IIa HDACs by TMP195 and TMP269 decreased intracellular *Mtb* outgrowth predominantly in Mϕ (**Figure 2B**). None of the compounds directly affected bacterial growth in liquid bacterial cultures while a suboptimal dose of the classical *Mtb* antibiotic rifampicin significantly inhibited *Mtb* (**Figure 2C**), confirming that HDAC inhibitors solely act via host-directed mechanisms and lack direct antimicrobial activity. Collectively, these data identify HDAC enzymes as a novel and important class of proteins in host regulatory networks that control intracellular bacterial survival. Furthermore, targeting HDACs with small molecules to regulate downstream inflammatory pathways could potentially be a novel host-directed therapeutic option for *Mtb* infections.

HDAC inhibition during differentiation polarizes macrophages into a more bactericidal phenotype.

Next, we investigated whether HDAC inhibitors could divert monocytes from the classical Mϕ1 and Mϕ2 differentiation pathways to cell subsets exhibiting distinct characteristics including an increased bactericidal phenotype. Monocytes were exposed to low concentrations of HDAC inhibitors during our standard GM-CSF driven Mϕ1 or M-CSF driven Mϕ2 differentiation protocol (**Figure 3A**). Macrophages differentiated in the presence of HDAC inhibitors were more effective in restricting intracellular bacterial growth in both Mϕ1 and Mϕ2 compared to DMSO control treated cells. The pan-HDAC inhibitor TSA was slightly more effective in controlling

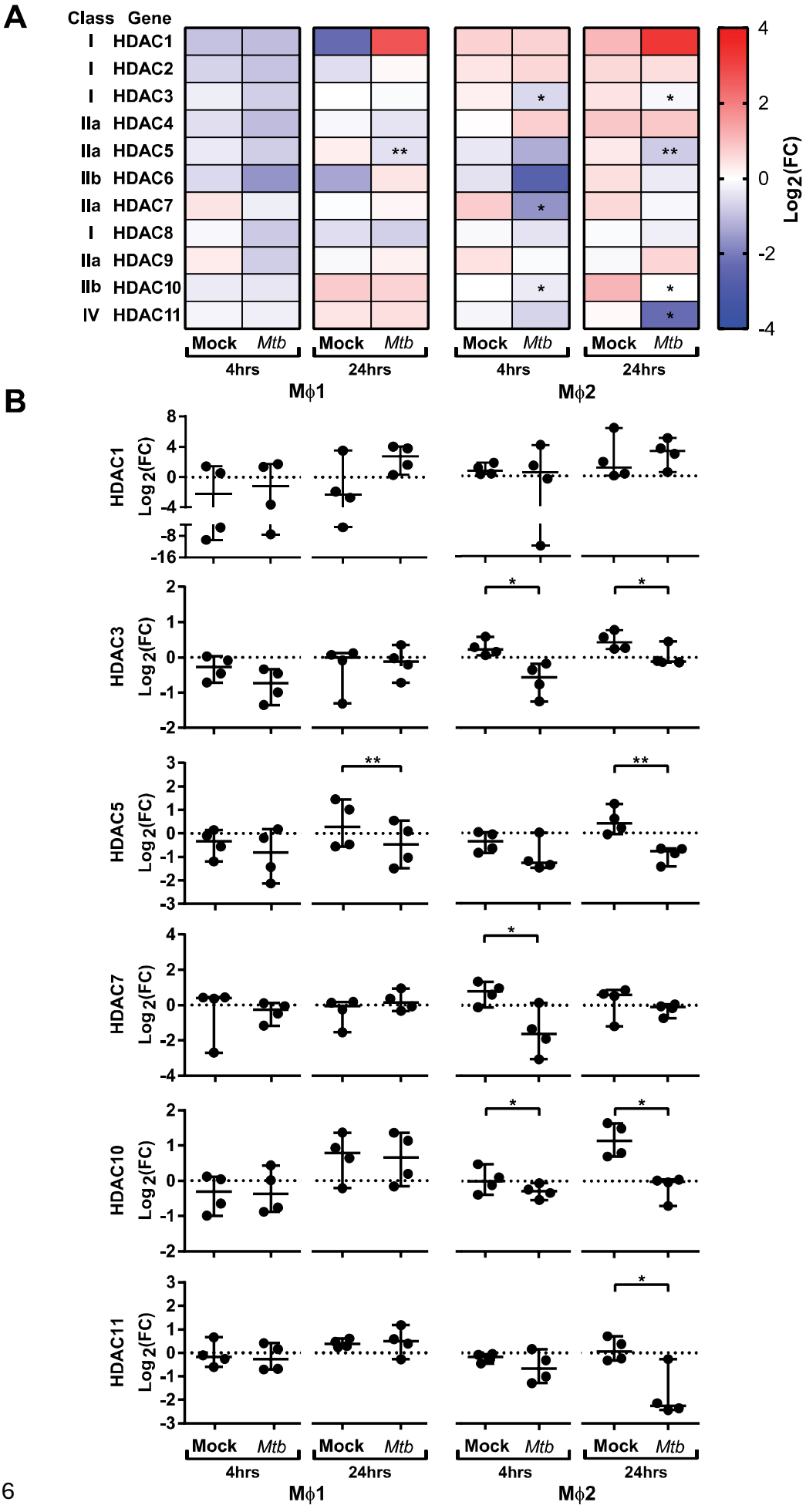
A
Class Gene
I HDAC1
I HDAC2
I HDAC3
IIa HDAC4
IIa HDAC5
IIb HDAC6
IIa HDAC7
I HDAC8
IIa HDAC9
IIb HDAC10
IV HDAC11
Mock Mtb
4hrs
24hrs
Mϕ1
Mϕ2
Log2(FC)
B
HDAC1
HDAC3
HDAC5
HDAC7
HDAC10
HDAC11

Figure 1. Expression kinetics of HDAC transcripts in primary human macrophages following Mtb infection.

Mϕ1 and Mϕ2 derived from 4 different donors were mock infected or infected with *Mtb* for 1h at MOI 10. Transcript levels of HDAC1-11 were determined in triplicate using qRT-PCR before (0h baseline) and 4 and 24h post-infection. Data was normalized to GAPDH (Ct) and mean expression levels of triplicate samples were calculated for each donor. A. Heatmap displaying median $\log_2$ fold changes (FC) of HDAC1-11 expression levels (pooled data of 4 donors) in response to *Mtb* infection compared to their respective baseline controls. B. Dot plots displaying log2 FC expression levels of HDAC1, 3, 5, 7, 10 and 11 in response to *Mtb* infection compared to their respective baseline controls, calculated using the formula $2^{-\Delta\Delta CT}$. Each dot represents a single donor. Horizontal lines indicate median log2 FC values of all 4 donors and whiskers represent 95% confidence intervals. Statistically significant differences compared to uninfected controls were tested using a paired sample t-test. (* = $p<0.05$, ** = $p<0.01$).

intracellular *Mtb* infection than the selective class IIa HDAC inhibitors TMP195 and TMP269 (**Figure 3B**, red dots). Importantly, the observed reduction in *Mtb* outgrowth in macrophages differentiated in the presence of HDAC inhibitors was not due to decreased cell viability (**Figure 3C**, red dots) or a diminished capacity to phagocytose (**Figure 3D**), implying a strongly increased intrinsic capacity to control intracellular bacterial survival. Of note, TMP195 consistently increased the phagocytic capacity as well as the percentage of phagocytic cells, especially in Mϕ1 (**Figure 3D** and **Supplementary Figure 2**), suggesting that the marginal reduction in bacterial load by Mϕ1 differentiated with TMP195 is considerably underestimating the increased bactericidal capacity induced by TMP195.

Since (1) upregulation of HDAC1 expression in *Mtb*-infected macrophages (**Figure 1**) has been postulated to involve the PKA-CREB-cJun signalling pathway [455] and (2) PKA inhibitor H-89 has previously been shown by us to counteract the manipulation of host signalling processes by *Mtb* [243, 296], we next investigated whether the restriction in bacterial outgrowth in macrophages differentiated in the presence of HDAC inhibitor could be further reduced by treating these macrophages subsequently with PKA inhibitors H-89 or 97i (an H-89 structural analogue) following *Mtb*-infection in Mϕ2 (**Figure 3B**, grey dots). Because the effect of HDAC inhibitors on *Mtb* bacterial survival was more prominent in Mϕ2 than Mϕ1 (**Figures 2B**), we additionally investigated the putative additive effect of HDAC and PKA host-directed compound combination in Mϕ2 only. As shown in **Figure 3F**, a clear additive effect was observed between HDAC and PKA inhibitors in Mϕ2 with the strongest reduction in bacterial load in 97i-treated TSA-

differentiated macrophages (median reduction of 69%), without resulting in significant toxicity (**Figure 3C**).

In summary, these data propose a key role for chromatin remodelling by histone acetylation in orchestrating host defence in TB. Thus, functional inhibition of HDACs may be a promising (host-directed) therapeutic addition to drug-combination regimens already in use for TB.

HDAC inhibition reduces bacterial burden *in vivo*.

To investigate the efficacy of HDAC inhibition *in vivo*, we employed a *Mycobacterium marinum* (*Mmar*) zebrafish embryo infection model. This model has been shown very effective for both fundamental and translational studies in the context of TB research [57, 300, 458, 459, 469]. Since treatment with HDAC inhibitor during human macrophage differentiation followed by infection showed the highest drug efficacy as described above, we translated the human *in vitro* model to *in vivo* zebrafish embryos by treating them starting at the 20 somite stage, at which the first macrophages appear [470]. At 24 hours post treatment, embryos were infected with *Mmar* and 3 days after infection, zebrafish embryos were imaged to quantify bacterial burden (**Figure 4A**). Both TMP195 and TSA pre-treatment reduced bacterial burden *in vivo*, with an average reduction of 37% and 32% respectively (**Figure 4B** and **4C**). Importantly, no developmental toxicity was observed. These *in vivo* results strongly support and strengthen our *in vitro* human macrophage results (**Figure 3B**).

HDAC activity regulates cytokine production by macrophages in response to *Mtb* infection.

Since HDAC activity has been implicated in guiding pro-versus anti-inflammatory responses, we evaluated whether exposure to low concentrations HDAC inhibitors during monocyte differentiation altered the phenotype of pro-inflammatory Mϕ1 and anti-inflammatory Mϕ2. Expression levels of cell surface markers discriminating between Mϕ1 and Mϕ2 (CD14, CD1a, CD163, CD11b) or monitoring the activation status of macrophages (CD80 and CD86) were not affected, except for CD14 whose expression level was upregulated in a proportion of TSA-differentiated Mϕ1 (**Supplementary Figure 3A**). Consistent with these findings, no morphological changes were observed in HDAC inhibitor-exposed Mϕ1 and Mϕ2 compared to DMSO controls (**Supplementary Figure 3B**).

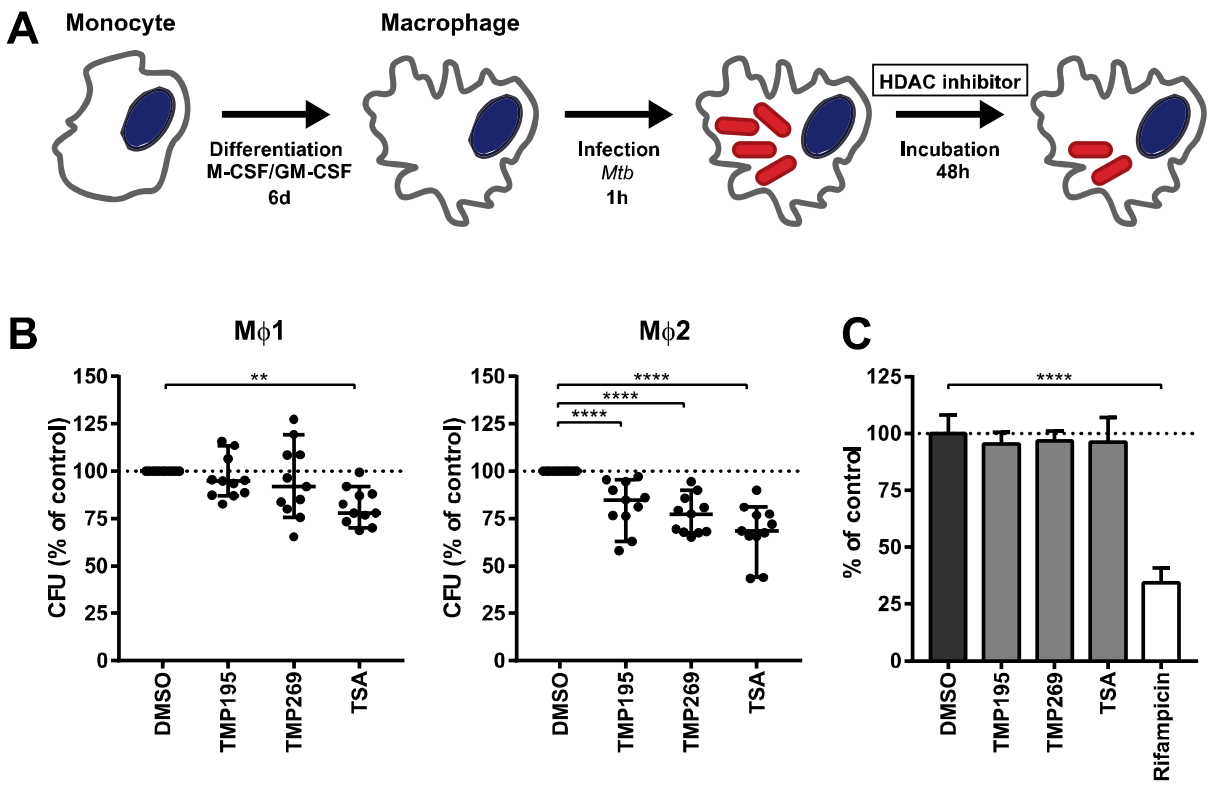

Figure 2. HDAC inhibitors decrease *Mtb* survival in human macrophages in a host-directed manner.

A. Schematic outline of the experimental setup used in (B). B. Mϕ1 and Mϕ2 macrophages derived from 11 different donors were infected with *Mtb* for 1h at MOI 10 and treated with TMP195 (10 µM), TMP269 (10 µM), TSA (100 nM) or DMSO at equal v/v for 48 hours post-infection. Dots represent the mean of 3 CFU assay replicates of a single donor expressed as a percentage of the DMSO control. Horizontal lines indicate median CFU values of all 11 donors and whiskers represent 95% confidence intervals. Statistically significant differences compared to DMSO were tested using a RM one-way ANOVA. (** = p<0.01, **** = p<0.0001). C. 13d treatment of a *Mtb* broth culture in the presence of 10 µM TMP195, TMP269 or TSA. Rifampicin (20 µg/ml) was used as a positive control. Bars depict the mean bacterial density at 550 nm ± standard deviation of six replicates from a representative experiment out of two independent experiments. The bacterial load is expressed as a percentage of the DMSO control value. Statistically significant difference compared to DMSO was tested using a one-way ANOVA with Dunnett's multiple test correction (**** = p<0.0001).

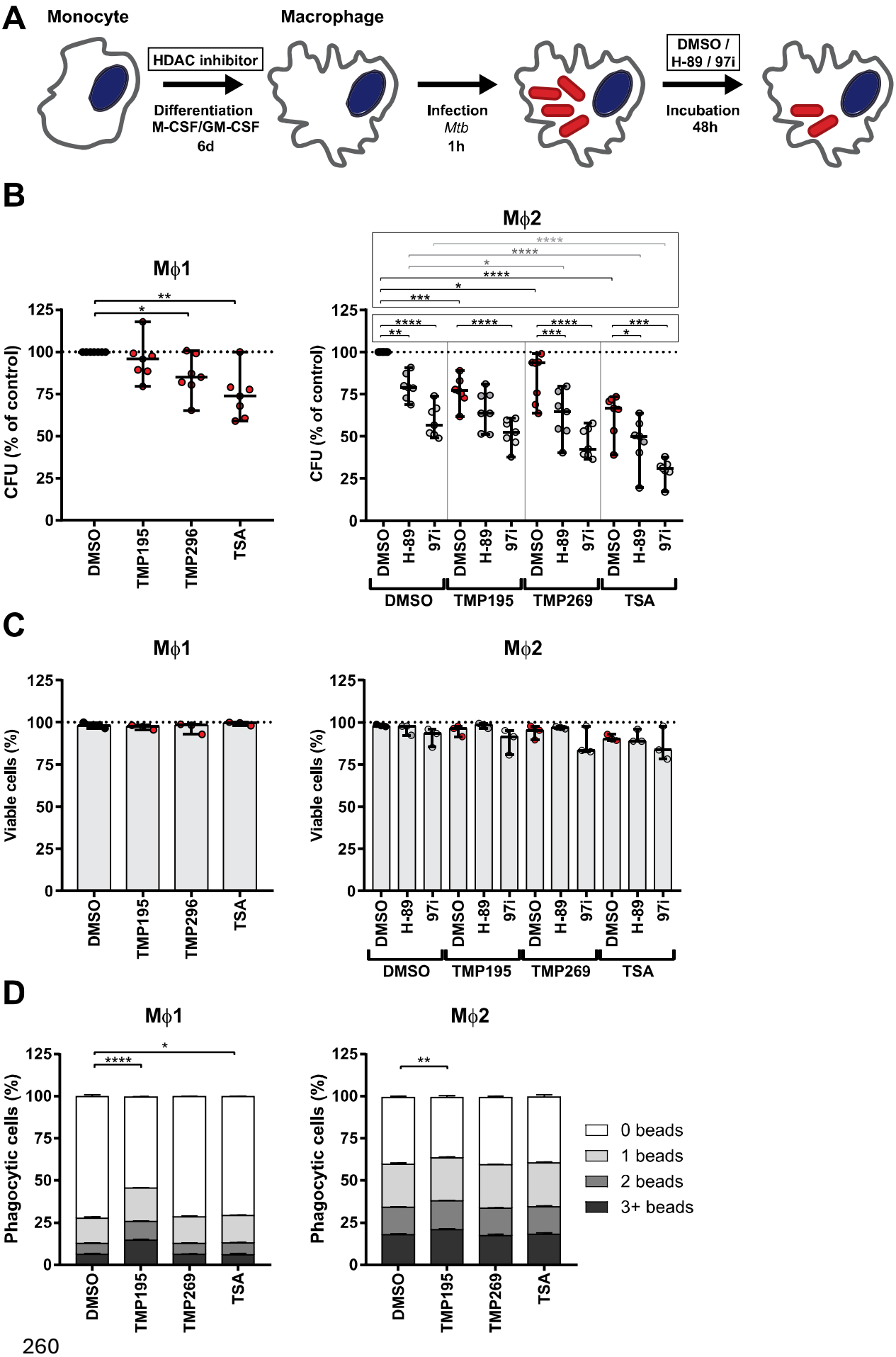
A
Monocyte
Macrophage
HDAC inhibitor
Differentiation
M-CSF/GM-CSF
6d
Infection
Mtb
1h
DMSO /
H-89 / 97i
Incubation
48h
B
Mϕ1
Mϕ2
CFU (% of control)
DMSO
TMP195
TMP296
TSA
H-89
97i
TMP269
C
Viable cells (%)
D
Phagocytic cells (%)
0 beads
1 beads
2 beads
3+ beads

Figure 3. Macrophages exposed during differentiation to low concentrations of HDAC inhibitors are more bactericidal.

A. Outline of the experimental setup used in (2B-D). B. Monocytes derived from 7 different donors were differentiated towards Mϕ1 and Mϕ2 while being exposed to TMP195 (300 nM), TMP269 (300 nM), TSA (30 nM) or DMSO at equal v/v for 6 days. Differentiated Mϕ1 and Mϕ2 were subsequently infected with *Mtb* for 1h at MOI 10 and incubated for 48 hours post-infection until readout. Dots represent the mean of 3 CFU assay replicates of a single donor expressed as a percentage of the DMSO control. Horizontal lines indicate median CFU values of all 7 donors and whiskers represent 95% confidence intervals. Statistically significant differences compared to DMSO were tested using a RM one-way ANOVA (* = p<0.05; ** = p<0.01; *** = p<0.001; **** = p<0.0001). C. Cell viability measurement of *Mtb*-infected Mϕ1 and Mϕ2 (experimental setup as in (B)). Dots represent the mean of 3 cell viability assay replicates of a single donor expressed as a percentage of the DMSO control. Bars indicate median values of all 3 donors and whiskers represent 95% confidence intervals. Statistically significant differences compared to DMSO were tested using a RM one-way ANOVA D. Phagocytic capacity of Mϕ1 and Mϕ2 was evaluated by flow-cytometry using fluorescent beads (experimental setup as in B). Macrophages were categorized into populations containing either 0, 1, 2 or 3+ beads. Bars depict mean ± standard deviation of 3 replicates. Data shown is 1 representative donor out of 4. Statistically significant differences compared to DMSO were tested using a one-way ANOVA with Dunnett's multiple test correction. (* = p<0.05; ** = p<0.01; **** = p<0.0001).

Before exploring whether exposure to low concentrations HDAC inhibitors during monocyte differentiation altered the cytokine/chemokine response of pro-inflammatory Mϕ1 and anti-inflammatory Mϕ2 upon *Mtb* infection, we first investigated the cytokine/chemokine responses of standardly differentiated Mϕ1 and Mϕ2 following infection with *Mtb*. Expression levels of 41 analytes were assessed in the supernatants of *Mtb*-infected Mϕ1 and Mϕ2 and compared to uninfected controls 24h after infection. Both anti-inflammatory cytokines (IL-10, IL-1ra) and pro-inflammatory cytokines (TNF-α, IL-6, GM-CSF, IL-1β, G-CSF, IL-12p40 and IL-17a) were upregulated in Mϕ1 and Mϕ2 but, as expected, the induction of pro-inflammatory cytokines was superior in Mϕ1 compared to Mϕ2 whereas the induction of anti-inflammatory cytokine IL-10 was highest in Mϕ2, confirming and extending our previous findings. (**Figure 5A** and **Supplementary Table 1**). To identify those cytokines/chemokines that highly discriminated between the innate responses of Mϕ1 and Mϕ2, a multilevel Partial Least Squares-Discriminant Analysis (PLS-DA) was performed. A PLS-DA rotates the PCA components to obtain maximal separation, producing Variable Importance in Projection (VIP) scores for each variable (e.g. analyte), reflecting the importance of each variable to the obtained separation (**Supplementary Figure 4A**). In parallel, the association of each cytokine/chemokine secretion level with either Mϕ1 or Mϕ2 24h after *Mtb* infection was calculated using Kendall's tau-b correlation test and plotted

against the VIP scores (**Figure 5C**). These combined analyses identified MDC, IL-1ra, GM-CSF, TNF-α and IL-12p40 as having moderate-to-strong correlations with *Mtb*-induced innate responses in Mϕ1, while for Mϕ2 MCP-1, IL-10, Eotaxin and GRO were either uncovered or confirmed.

Next, we investigated the effect of exposure to low dose HDAC inhibitors during monocyte differentiation on the cytokine/chemokine response of Mϕ1 and Mϕ2 following *Mtb* infection (**Figure 5B** and **Supplementary Table 1**). Exposure to pan-HDAC inhibitor TSA and class IIa HDAC inhibitors TMP195 and TMP269 potently dampened the production of both anti- and pro-inflammatory cytokines as well as the majority of chemokines tested in Mϕ1 in response to *Mtb* infection. In contrast, exposure to HDAC inhibitors during differentiation had limited impact on the innate response of Mϕ2 with several cytokines/chemokines being slightly lowered in their production while the production of others was only marginally enhanced. To identify cytokines/chemokines most strongly associated with HDAC inhibition, PLS-DA analyses were performed separately for Mϕ1 and Mϕ2 and Kendall's correlation coefficients were calculated for every HDAC inhibitor-induced cytokine/chemokine response (**Figure 5D** and **Supplementary Figure 4B**). In Mϕ1, G-CSF and IFN-γ displayed a clear negative correlation with pan-HDAC and selective class IIa HDAC inhibition, while IL-6, MCP-1 and MIP-1α showed a negative correlation specifically with class IIa inhibition. In contrast, only weak correlations were observed for Mϕ2 (except for MIP-1α, IL-1β, and IL-8 upon TMP269 exposure), confirming a limited effect of exposure to low concentrations HDAC inhibitors during differentiation towards Mϕ2 on cytokines/chemokines responses following infection with *Mtb*.

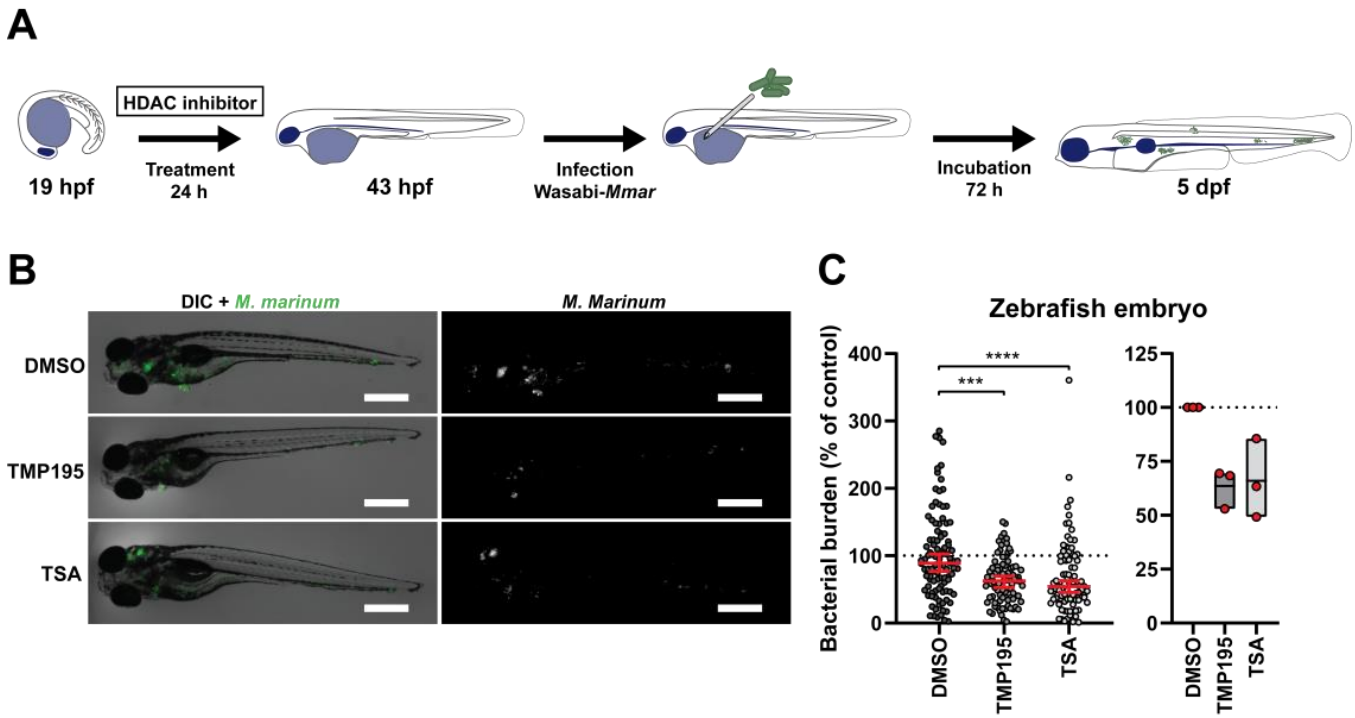

Figure 4. Zebrafish embryos exposed to HDAC inhibitors display reduced bacterial burden.

A. Outline of the experimental setup used in (4B-C). B. Zebrafish embryos were at 19 hours post fertilization (hpf), i.e. the 20 somite stage, exposed to TMP195 (10 μM), TSA (30 nM) or the solvent, DMSO, at equal v/v for 24 hours. Embryos were subsequently infected by microinjection of 250-300 CFU *Mycobacterium marinum* (*Mmar*) expressing Wasabi fluorescent protein, into the Duct of Cuvier. Infected larvae imaged for *Mmar* fluorescence at 3 days post infection. Images shown are representative images of each treatment group. Scale bar indicates 500 μm. C. Bacterial burden of all zebrafish larvae (left panel) or each independent experiment (right panel) (experimental setup as in (A)). Graphs represent zebrafish larvae from different parent couples used in 3 independent experiments, and treated with TMP195 (n=92), TSA (n=90) or DMSO at equal v/v (n=102) expressed as a percentage of the DMSO control. Each dot indicates an embryo with whiskers in red representing median with 95% confidence intervals (left panel) or each dot indicates the mean of a single experiment with floating bars representing min. to max. with mean of the 3 independent experiments.

To investigate whether mRNA levels correlated with decreased cytokine and chemokine secretion, mRNA levels encoding 8 molecules whose secretion changed in response to HDAC inhibition (**Figure 5B** and **5D**), were measured using qPCR in Mϕ1 since they showed the most profound changes (**Supplementary Figure 4C**). For CCL2 (MCP-1) and CCL4 (MIP-1β), a clear correlation with chemokine secretion levels was found, in contrast to CXCL8 (IL-8) and CCL3 (MIP-1α). For some cytokines, IL-6, G-CSF and IFN-γ, that were secreted in low amounts (median secretion below 100 pg/ml) we could not detect decreases in mRNA levels. Surprisingly, TNF could not be detected

despite the fact that secretion of TNF-α levels were found that exceeded 1 μg/ml which suggests that post transcriptional regulation plays a major role in TNF translation. Because both G-CSF and IFN-γ negatively correlated with HDAC inhibition in *Mtb*-infected Mϕ1 and IFN-γ is known to play a major role in TB pathogenesis [471], we further explored the possible role of IFN-γ. Interestingly, IFN-γ addition decreased the efficacy of HDAC inhibition in Mϕ1 (**Supplementary Figure 5B**), without affecting cell viability (**Supplementary Figure 5C**). To investigate whether IFN-γ treatment could impact HDAC expression, expression levels of HDAC1 and HDAC5, whose expression levels were affected most in Mϕ1 (**Figure 1**), were quantified upon *Mtb*-infection of different Mϕ1. No differences were found between the *Mtb*-infected Mϕ1 for both HDAC1 and HDAC5 (**Supplementary Figure 5D**), but in the presence of IFN-γ a large downregulation of HDAC1 mRNA was observed for Mϕ1 differentiated in the presence of TSA (**Supplementary Figure 5E**). Together with its strong upregulation upon infection (**Figure 1** and **Supplementary Figure 1**), this supports an important role for HDAC1 in infection.

Collectively, HDAC inhibition during macrophage differentiation profoundly downregulated inflammatory cytokine production induced by *Mtb* infection, particularly in Mϕ1. For some chemokines, this clearly correlated with lowered mRNA levels while this correlation was absent for others, suggesting post-transcriptional modification also plays a role. Since *Mtb* can exploit host cytokine signalling networks for its survival and a delicate balance between pro- and anti-inflammatory cytokines is required to restrict *Mtb* proliferation [472], these data suggest that HDACs may affect the outcome of *Mtb* infection by altering infection-induced orchestrated cytokine/chemokine responses by innate immune cells.

Discussion

Here, we report that histone deacetylase (HDAC) transcriptomic levels are strongly affected by *Mtb*-infection in primary human macrophages. Secondly we report that broad chemical HDAC inhibition can enhance the antimicrobial response of both Mϕ1 and Mϕ2, while selective inhibition of class IIa HDACs prominently decreased bacterial outgrowth in Mϕ2. Thirdly, chemical inhibition of HDAC activity during differentiation polarized macrophages into a more bactericidal phenotype with a concomitant decrease in the secretion levels of inflammatory cytokines. Fourth, *in vivo* chemical inhibition of HDAC activity in *Mycobacterium marinum* infected zebrafish embryos, a well characterized animal model for tuberculosis, significantly reduced mycobacterial burden *in vivo*, validating our *in vitro* findings in primary human macrophages. Collectively, these data identify HDACs as druggable host targets for HDT against intracellular *Mtb*.

Previous studies have suggested that *Mtb* can modulate host defence by epigenetic modifications to facilitate survival within the host cell [454-456]. In this study, we observed that following *Mtb* infection, transcriptional levels of several HDACs representing different classes were differentially regulated in Mϕ1 but primarily in Mϕ2. Our findings, which are in agreement with (in this paper) independently analyzed results from Blischak, Tailleux [467], identify HDAC enzymes as potential targets for immune modulation in infectious diseases. This idea is supported by similar expression levels for several HDACs compared to uninfected when Mϕ2 were infected with a virulent *Mtb* strain. Since macrophage differentiation states are known to be dynamic and flexible, macrophages represent highly interesting therapeutic targets, both in differentiated (e.g. Mϕ1 and Mϕ2) and in less differentiated stages. Interestingly, treatment with the pan-HDAC inhibitor TSA decreased bacterial survival in both *Mtb*-infected Mϕ1 and Mϕ2 while selective class IIa HDAC inhibitors TMP195 and TMP269 decreased *Mtb* survival predominantly in Mϕ2. This is one of the first studies comparatively analyzing HDT in Mϕ1 and Mϕ2 in a human infection model, indicating that downregulation of HDAC activity in the context of *Mtb* infection can be beneficial to host control of infection. The attenuated efficacy of class IIa HDAC inhibitors on *Mtb* survival in Mϕ1 might be explained by the lower basal expression levels of HDAC5 and HDAC7 in Mϕ1 compared to Mϕ2 (**Supplementary Figure 1A**), which could suggest that the therapeutic window of these inhibitors is significantly larger in Mϕ2.

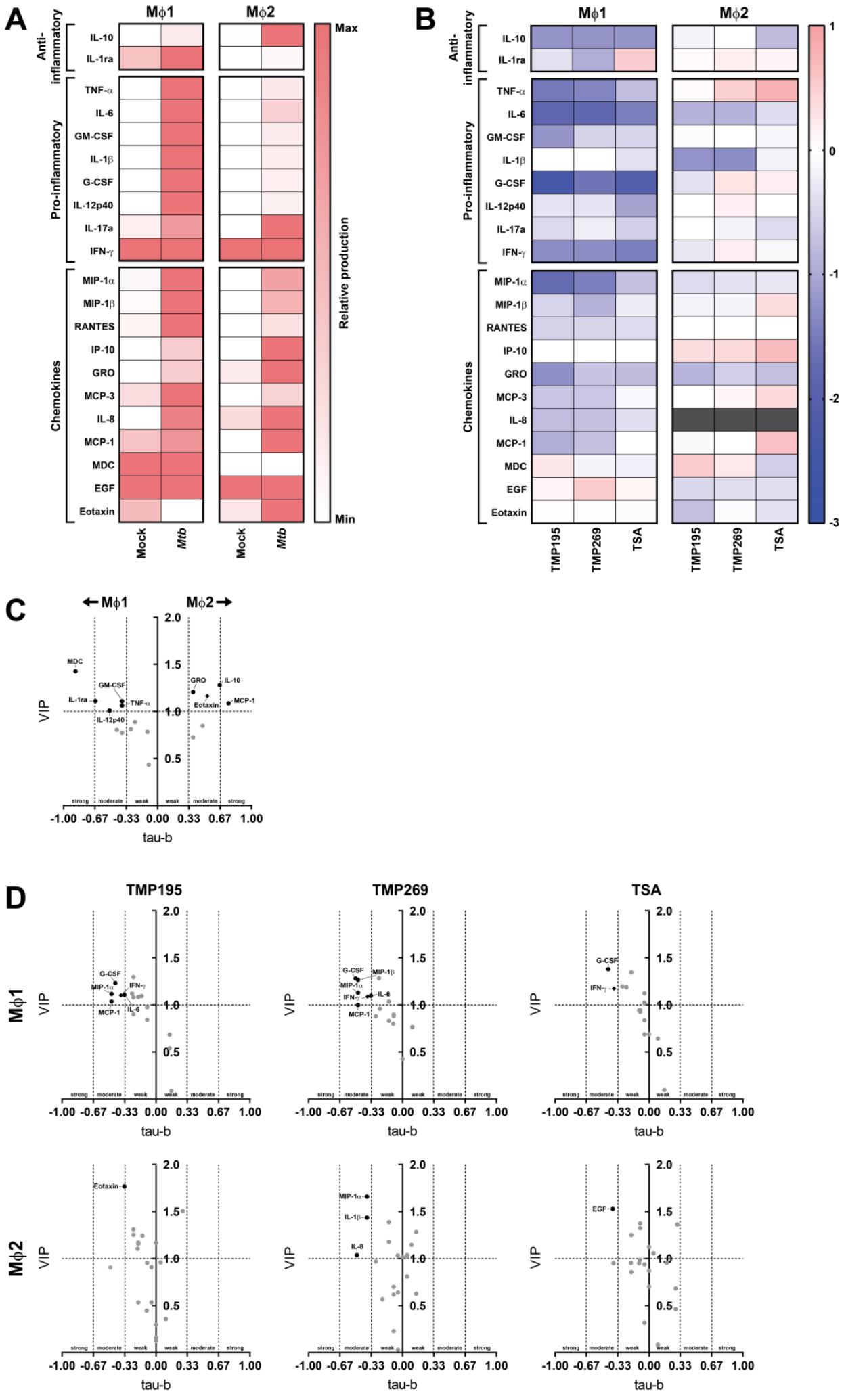
A
Mϕ1
Mϕ2
Anti-inflammatory
Pro-inflammatory
Chemokines
IL-10
IL-1ra
TNF-α
IL-6
GM-CSF
IL-1β
G-CSF
IL-12p40
IL-17a
IFN-γ
MIP-1α
MIP-1β
RANTES
IP-10
GRO
MCP-3
IL-8
MCP-1
MDC
EGF
Eotaxin
Max
Min
Relative production
Mock
Mtb
B
TMP195
TMP269
TSA
1
0
-1
-2
-3
C
← Mϕ1
Mϕ2 →
VIP
tau-b
strong
moderate
weak
D
TMP195
TMP269
TSA
Mϕ1
Mϕ2
VIP
tau-b

Figure 5. Exposure to low concentrations HDAC inhibitors during monocyte differentiation alters the cytokine/chemokine response of Mϕ1 and Mϕ2 upon *Mtb* infection.

A. Heat map displaying median cytokine/chemokine expression levels (of 4 different donors) in supernatants of standardly differentiated Mϕ1 and Mϕ2 24h following *Mtb* or mock infection. Each row represents the relative expression of the indicated cytokine/chemokine using a white to red colour scale. Of the 41 analytes measured, only cytokines/chemokines that changed in at least 3 out of 4 donors and exhibited a minimal median $\log_2$ fold change (FC) of 0.5 in a single comparison are shown. **B.** Heat map displaying median $\log_2$ FC of cytokine/chemokine levels in supernatants of Mϕ1 and Mϕ2 of 4 different donors. In this experimental setup monocytes were exposed to TMP195 (300 nM), TMP269 (300 nM), TSA (30 nM) or DMSO at equal v/v during differentiation towards Mϕ1 and Mϕ2. Gray color depicts cytokine/chemokine levels that were detected above the linear range of the assay. **C.** Experimental setup as in (A). Variable Importance in Projection (VIP) scores of the first x-variate were extracted from each PLS-DA analysis and cytokine values equal or greater than 1 were considered relevant. In parallel, Kendall's tau-b correlation coefficients were calculated for each cytokine. Coefficients between 0-0.33, 0.33-0.67 and 0.67-1 were considered to have a weak, moderate and strong correlation, respectively. Every dot represents a cytokine/chemokine. Cytokines/chemokines with a VIP score >1 and demonstrating at least a moderate correlation are annotated in black. Annotated cytokines that were produced below or equal to a median concentration of 40 pg/ml are depicted by a diamond. **D.** Experimental setup as in (B). VIP scores and Kendall's tau-b correlation coefficients calculations as in (C).

A recent cohort study in Uganda compared whole genome transcriptional profiles of *Mtb*-infected monocytes derived from peripheral blood of household contacts of TB patients who were resistant to *Mtb* infection (resisters) with individuals who were susceptible to *Mtb* infection (latent TB infection (LTBI)) [473, 474]. Consistent with our observation that histone deacetylase function is important for the innate immune response to *Mtb* infection, they showed that pathways controlled by histone deacetylases were markedly differentially activated between the two study groups. The clinical potential of HDAC inhibition in the context of TB has already been proven by studies showing reduced bacterial burden in an *in vivo* mouse model using Tubustatin A, a HDAC6 inhibitor [193]. Here, we significantly expand upon this work by demonstrating the potential of both a selective class IIa inhibitor and a pan-HDAC inhibitor, TMP195 and TSA respectively, for treating mycobacterial infection in an *in vivo* model. Zebrafish embryos pre-treated with TMP195 or TSA, at concentrations not inducing developmental toxicity, showed a clear reduction in mycobacterial infection burden. A useful characteristic of the *Mmar* zebrafish embryo infection model is the lack of functional adaptive immune cells, thus allowing the assessment of innate immunity only [475]. Despite the absence of T-cells, macrophage aggregates with

granuloma-like features nevertheless are formed, a critical feature of TB [386]. Therefore, our results support the effectivity of HDAC inhibitors during early stages of TB granuloma formation. Future work should be directed towards dissecting the effect of these HDT compounds in the presence of adaptive immunity and mature TB granulomas. Future work should be directed towards dissecting the effect of these HDT compounds in the presence of adaptive immunity. Collectively, the independent data sets reported in our study and by others [193] strongly suggest that HDACs are an important factor in the innate immune response to *Mtb* infection, and that their inhibition can enhance antimicrobial activity of infected macrophages.

Interestingly, we found that targeting HDACs in monocytes during differentiation to either Mϕ1 or Mϕ2 strongly improved the ability of the host to control subsequent *Mtb* infection. In agreement with our finding, Guerriero *et al*, demonstrated in an *in vivo* mouse cancer model that treatment with class IIa HDAC inhibitor TMP195 increased the anti-tumour potential of macrophages by pharmacologic modulation of the macrophage phenotype [461]. Importantly, in our *in vitro Mtb*-macrophage infection model, a combinatorial regimen of HDAC and PKA/PKB inhibitors resulted in a clearly additive effect in decreasing intracellular bacterial survival in Mϕ2 (Figure 3B). The PKA/PKB inhibitor H-89 has been shown to regulate a kinase network around AKT1/PKB-AS160-RAB14 that controls the intracellular survival of *Mtb* and *Salmonella* by manipulating phagosome maturation and actin remodelling [243, 296]. Furthermore, PKA is known to be involved in numerous other signalling pathways associated with *Mtb* survival [476, 477]. Moreover, PKA inhibition might also have impaired class IIa HDAC function by interfering with nucleocytoplasmic trafficking since PKA activation promotes nuclear import of HDAC4 by phosphorylation and inhibits class IIa HDAC nuclear export via the LKB1-SIK2/3 axis [478, 479]. Demonstration of synergistic effects of TSA and PKA/PKB inhibitors is in line with results by Zhu, Cai [480], who demonstrated upregulation of the PI3K-AKT1 signalling pathway in *Mtb*-infected THP-1 cells treated with TSA. Of note, Zhu, Cai [480] reported TSA to promote *Mtb* survival but this discrepancy is likely explained by the use of the THP-1 cell line which requires stimulation with phorbol 12-myristate 13-acetate (PMA) as opposed to primary macrophages, as well as the higher concentration (625 nM) of TSA they used, which was highly toxic in our model. Our work is one of the first demonstrations of synergism [481] between different HDT compounds in the control of bacterial pathogens and provides an important avenue for further studies in this area. We speculate that the simultaneous targeting of mechanistically different host pathways underlies this synergism.

The kinetics and quantities of cytokines released by the host during infection is an important aspect influencing the outcome of immune responses against *Mtb* [472,

482]. Surprisingly, while HDAC inhibition during monocyte differentiation restricted intracellular bacterial outgrowth more effectively in *Mtb*-infected Mϕ2 than Mϕ1 (Figure 3B), the cytokine/chemokine secretion profile was only moderately altered in Mϕ2 (Figure 4B). In contrast, Mϕ1 exposed during differentiation to HDAC inhibitors clearly displayed a less pro-inflammatory phenotype, raising the question which HDAC inhibitor-induced cytokine/chemokine profile is optimal for host resistance against *Mtb*. In line with this, the addition of IFN-γ, a protein known to be vital in TB pathogenesis [471], impaired the effect of HDAC inhibition on bacterial survival in Mϕ1. Lastly, TSA-enhanced Mϕ2 polarization was demonstrated to be dependent on TSA-induced autophagy [483], a process vital for the clearance of *Mtb* [484]. Future work will need to explore the role of autophagy in *Mtb*-infected macrophages treated with HDAC inhibitors.

Interestingly, it has been shown that both silencing and chemical inhibition of class IIa HDACs induces the expression of transcription factor Nur77, an orphan nuclear receptor and immediate-early gene that regulates cellular proliferation, apoptosis, inflammation, and glucose metabolism [485]. Nur77 has been demonstrated to promote anti-inflammatory function by rewiring the tricarboxylic acid (TCA) cycle in pro-inflammatory macrophages [486]. Moreover, Nur77-deficiency was found to drive macrophage polarization towards a pro-inflammatory phenotype, characterized by increased IL-6, IL-12 and IFN-γ production, among others [487, 488]. Despite the fact that specific effects of different HDACs on inflammatory profiles are just beginning to be elucidated (**Supplementary Table 2**), we hypothesize that modulation of cytokine/chemokine secretion is a likely mechanism by which *Mtb* can evade from host defence and propose that this may be therapeutically counteracted by inhibiting HDAC-mediated transcriptional regulation [472].

Although HDAC inhibitors are well known for their regulation of transcriptional activity by histone deacetylation, their function may not be limited to modulating epigenetic changes. For example, it has been shown by Grégoire *et al* that the function of transcription factor MEF2 can be inhibited through class IIa HDAC-mediated sumoylation [489, 490]. Regulation of these alternative functions may also have contributed to an enhanced bactericidal capacity of HDAC inhibitor-treated macrophages. Therefore, a more complete understanding of the complex function of HDAC enzymes and their effect on cellular and immuno-modulatory processes will be necessary to understand the full therapeutic potential of their inhibitors.

In summary, our findings demonstrate that HDAC inhibitors offer the possibility to augment antimicrobial responses against *Mtb* infection. Moreover, they can act in synergy with other host-directed strategies and may well synergize also with current

antibiotics to improve TB treatment efficacy and to shortening TB therapies, a major goal in TB research. Although exploitation of HDACs as druggable targets for HDT against intracellular *Mtb* requires further work, our data clearly suggest that pharmacological targeting of host epigenetic regulation could be a promising strategy to improve the innate immune response against *Mtb*.

Supplementary Figures

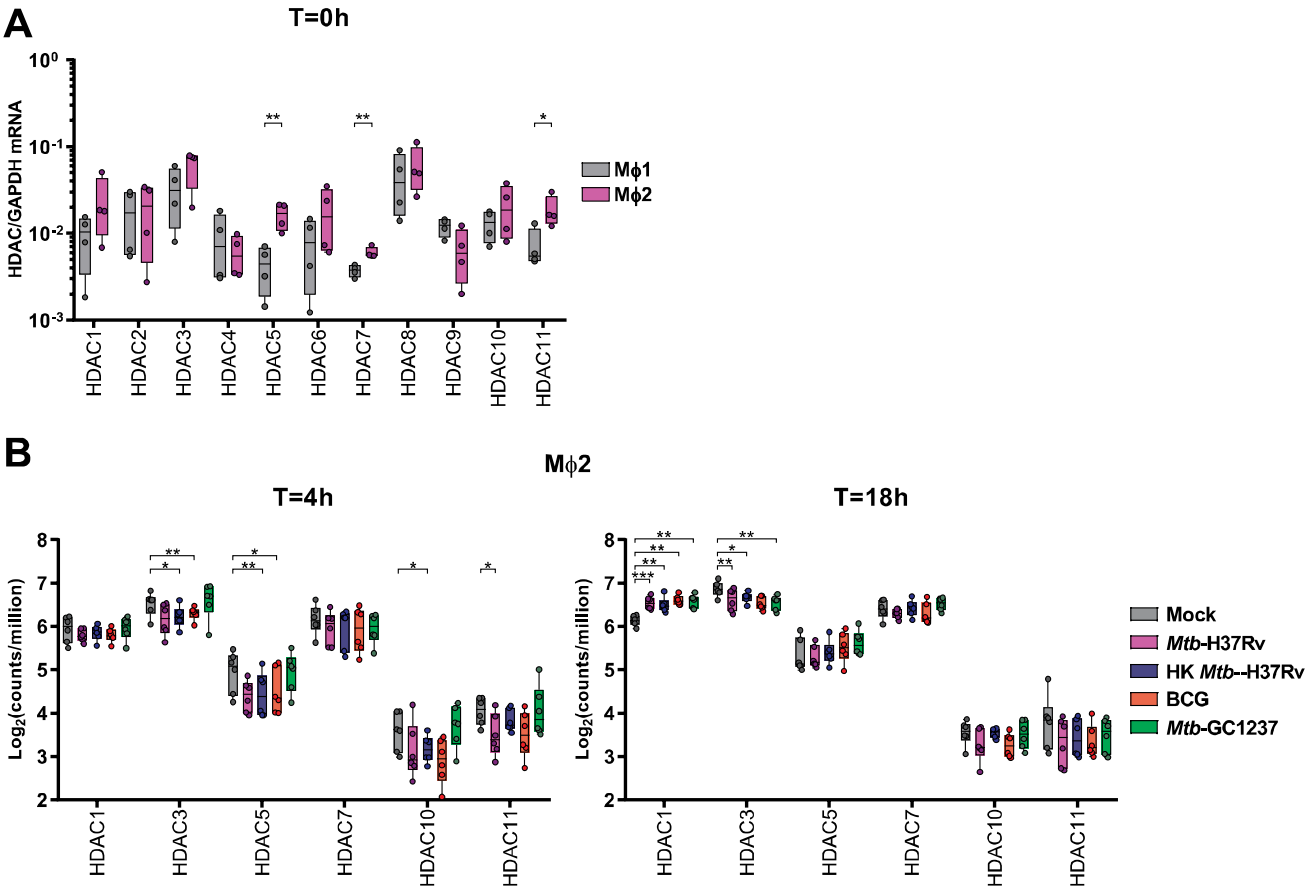

Supplementary Figure 1. Validation of HDAC transcriptomic profiles in primary human macrophages following Mtb infection.

A. Basal transcript levels of HDAC1-11 were determined in triplicate using qRT-PCR analysis at baseline (0h) in Mϕ1 and Mϕ2 derived from 4 different donors. Data was normalized to GAPDH ($(2^{-\Delta Ct(HDAC)})/(2^{-\Delta Ct(GAPDH)})$) and mean expression levels of triplicate samples were calculated for each donor. Box-and-whisker plots (min to max) show gene expression levels of the 4 donors where each dot represents a single donor. Significant differences between macrophage subsets were determined using a paired sample t-test. B. HDAC expression levels were extracted from a published RNA-sequencing dataset of infected Mϕ2 [467]. Mϕ2 of 6 different donors were mock infected or infected for 1h at MOI 2 with either *Mtb*-H37Rv, heat-killed *Mtb*-H37Rv, bacillus Calmette-Guérin (BCG) or *Mtb*-GC1237 and RNA was isolated 4 and 18h post-infection. Box-and-whisker plots (min to max) display the median $\log_2$ counts per million of the 6 donors and each dot represents a single donor. Statistically significant differences compared to uninfected controls were tested using a repeated measure (RM) one-way ANOVA with Dunnett's multiple test correction. (* = $p<0.05$, ** = $p<0.01$ and *** = $p<0.001$).

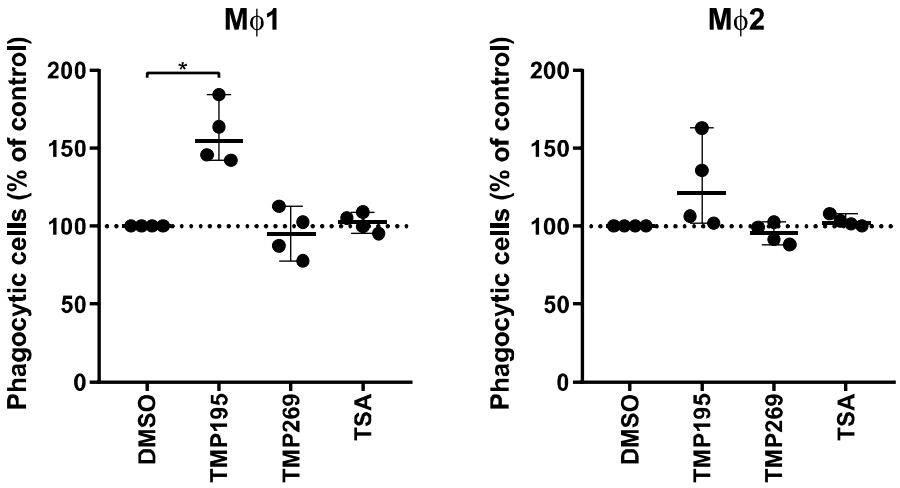

Supplementary Figure 2. A higher percentage of macrophages exhibit phagocytic capabilities when exposed during differentiation to low concentrations of HDAC inhibitor TMP195.

The percentage of Mϕ1 and Mϕ2 with phagocytic capabilities (containing 1+ beads) was evaluated by flow-cytometry using fluorescent beads (experimental setup as in Fig 3D). Dots represent the mean of 3 replicates of a single donor expressed as a percentage of the DMSO control. Horizontal lines indicate median percentage phagocytic cells of all 4 donors and whiskers represent 95% confidence intervals. Statistically significant differences compared to DMSO were tested using a RM one-way ANOVA with Dunnett's multiple test correction. (* = $p<0.05$).

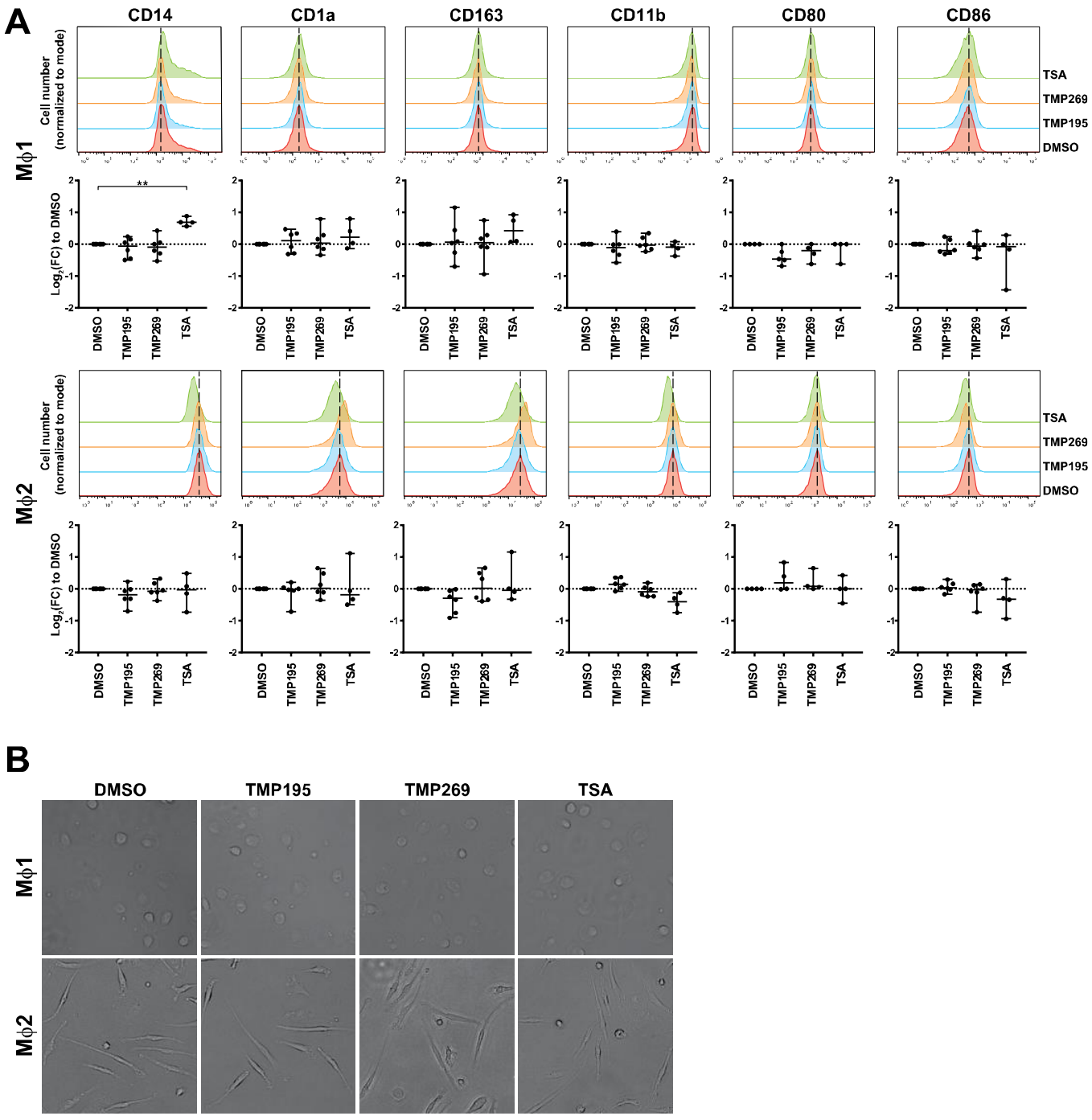

Supplementary Figure 3. Expression of cell surface markers is unaltered on macrophages exposed to low concentrations of HDAC inhibitors during differentiation.

Monocytes derived from 4-6 different donors were differentiated towards Mϕ1 and Mϕ2 while being exposed to TMP195 (300 nM), TMP269 (300 nM), TSA (30 nM) or DMSO at equal v/v for 6 days. **A.** Histograms depicting fluorescent intensities of cell surface markers (Top panel). For each cell surface marker the geometric mean fluorescent intensities (GMI) were calculated per donor. Dots represent the median log2 fold changes (FC) in response to chemical inhibition of HDAC activity during monocyte differentiation and is expressed as a percentage of the DMSO control. Horizontal lines indicate median fluorescent intensity values of all 4-6 donors and whiskers represent 95% confidence intervals. Statistically significant differences compared to DMSO were tested using a RM one-way ANOVA (** = $p<0.01$) (Lower panel). **B.** Bright field microscopy images showing the morphology of Mϕ1 and Mϕ2 exposed to TMP195 (300 nM), TMP269 (300 nM), TSA (30 nM) or equivalent volume of DMSO during differentiation (magnification 200x).

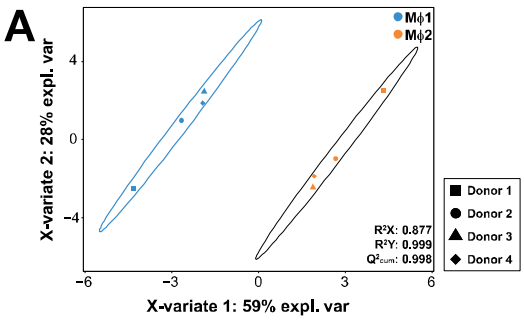
A
Mϕ1
Mϕ2
X-variate 2: 28% expl. var
X-variate 1: 59% expl. var
R²X: 0.877
R²Y: 0.999
Q²cum: 0.998
Donor 1
Donor 2
Donor 3
Donor 4

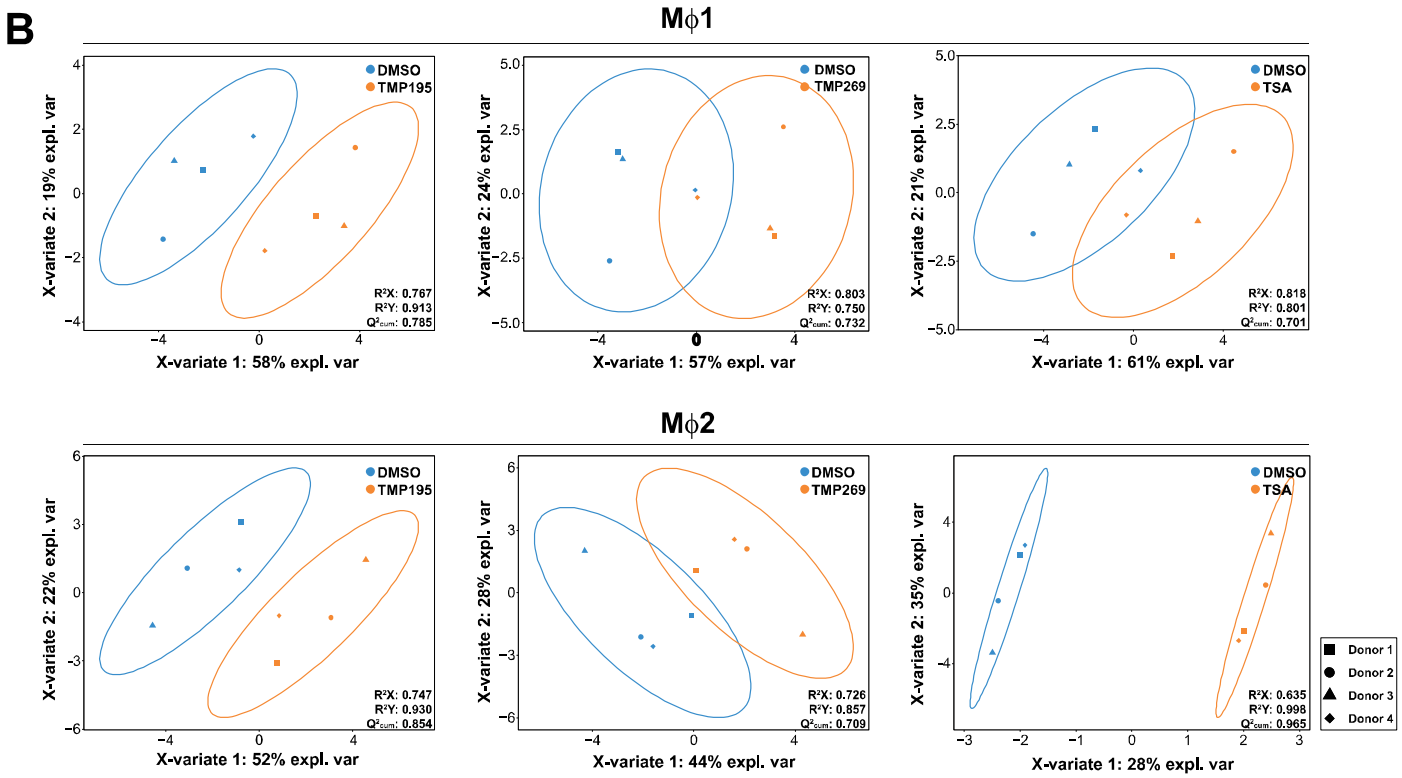
B
Mϕ1
DMSO
TMP195
X-variate 2: 19% expl. var
X-variate 1: 58% expl. var
R²X: 0.767
R²Y: 0.913
Q²cum: 0.785
DMSO
TMP269
X-variate 2: 24% expl. var
X-variate 1: 57% expl. var
R²X: 0.803
R²Y: 0.750
Q²cum: 0.732
DMSO
TSA
X-variate 2: 21% expl. var
X-variate 1: 61% expl. var
R²X: 0.818
R²Y: 0.801
Q²cum: 0.701
Mϕ2
DMSO
TMP195
X-variate 2: 22% expl. var
X-variate 1: 52% expl. var
R²X: 0.747
R²Y: 0.930
Q²cum: 0.854
DMSO
TMP269
X-variate 2: 28% expl. var
X-variate 1: 44% expl. var
R²X: 0.726
R²Y: 0.857
Q²cum: 0.709
DMSO
TSA
X-variate 2: 35% expl. var
X-variate 1: 28% expl. var
R²X: 0.635
R²Y: 0.998
Q²cum: 0.965
Donor 1
Donor 2
Donor 3
Donor 4

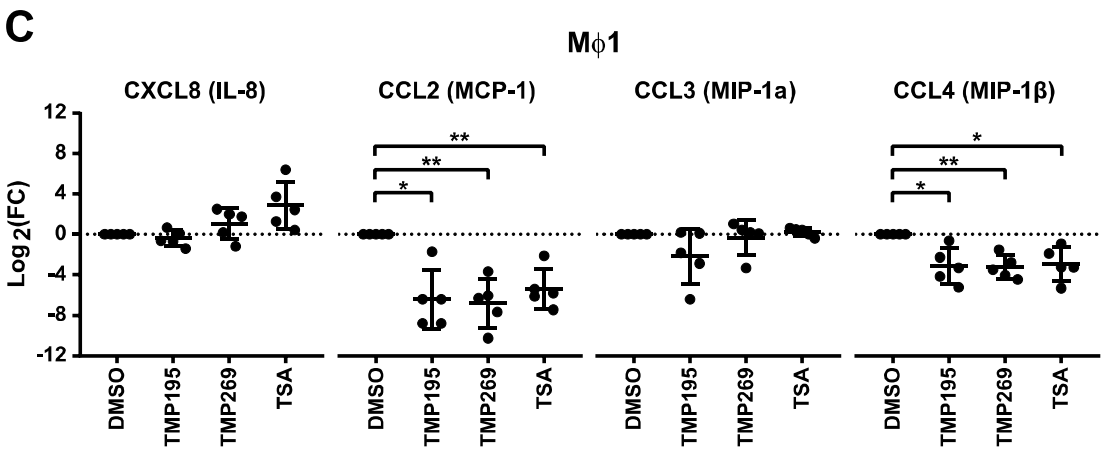
C
Mϕ1
CXCL8 (IL-8)
CCL2 (MCP-1)
CCL3 (MIP-1a)
CCL4 (MIP-1β)
Log 2(FC)
DMSO
TMP195
TMP269
TSA

Supplementary Figure 4. Inhibition of HDAC activity during monocyte differentiation modifies the cytokine/chemokine response of Mϕ1 and Mϕ2 upon Mtb infection.

A. A multilevel PLS-DA model of cytokine profiles derived from standardly differentiated Mϕ1 and Mϕ2 24h following *Mtb* infection was generated using R package mixOmics. Model validity is indicated by the R^2X, R^2Y and Q^2_{cum} scores. B. Multilevel PLS-DA models of cytokine profiles derived from *Mtb*-infected Mϕ1 and Mϕ2 exposed to TMP195 (300 nM), TMP269 (300 nM), TSA (30 nM) or DMSO at equal v/v during differentiation were generated using R package mixOmics. Model validity is indicated by the R^2X, R^2Y and Q^2_{cum} scores. C. Quantification of cytokine/chemokine mRNA levels in primary human Mϕ1 following 24 hours of *Mtb* infection. Experimental setup as in B. mRNA levels of the genes TNF (TNF-α), IL6 (IL-6), CSF3 (G-CSF), IFNG (IFNG-γ), CCL3 (MIP-1α), CCL4 (MIP-1β), CXCL8 (IL-8) and CCL2 (MCP-1) were determined in duplicate using qRT-PCR analysis in Mϕ1 derived from 5 different donors. Data was normalized to GAPDH (□Ct) and mean expression levels of duplicate samples were calculated for each donor. Dot plots display log2 FC expression levels of CXCL8, CCL2, CCL3 and CCL4 to their respective baseline controls which is standardly differentiated Mϕ1, calculated using the formula $2^{-\Delta\Delta CT}$. Each dot represents a single donor where horizontal lines indicate median log2 FC values of all 5 donors and whiskers represent 95% confidence intervals. Significant differences between macrophage subsets were determined using a RM one-way ANOVA with Dunnett's multiple test correction. (* = $p<0.05$ and ** = $p<0.01$).

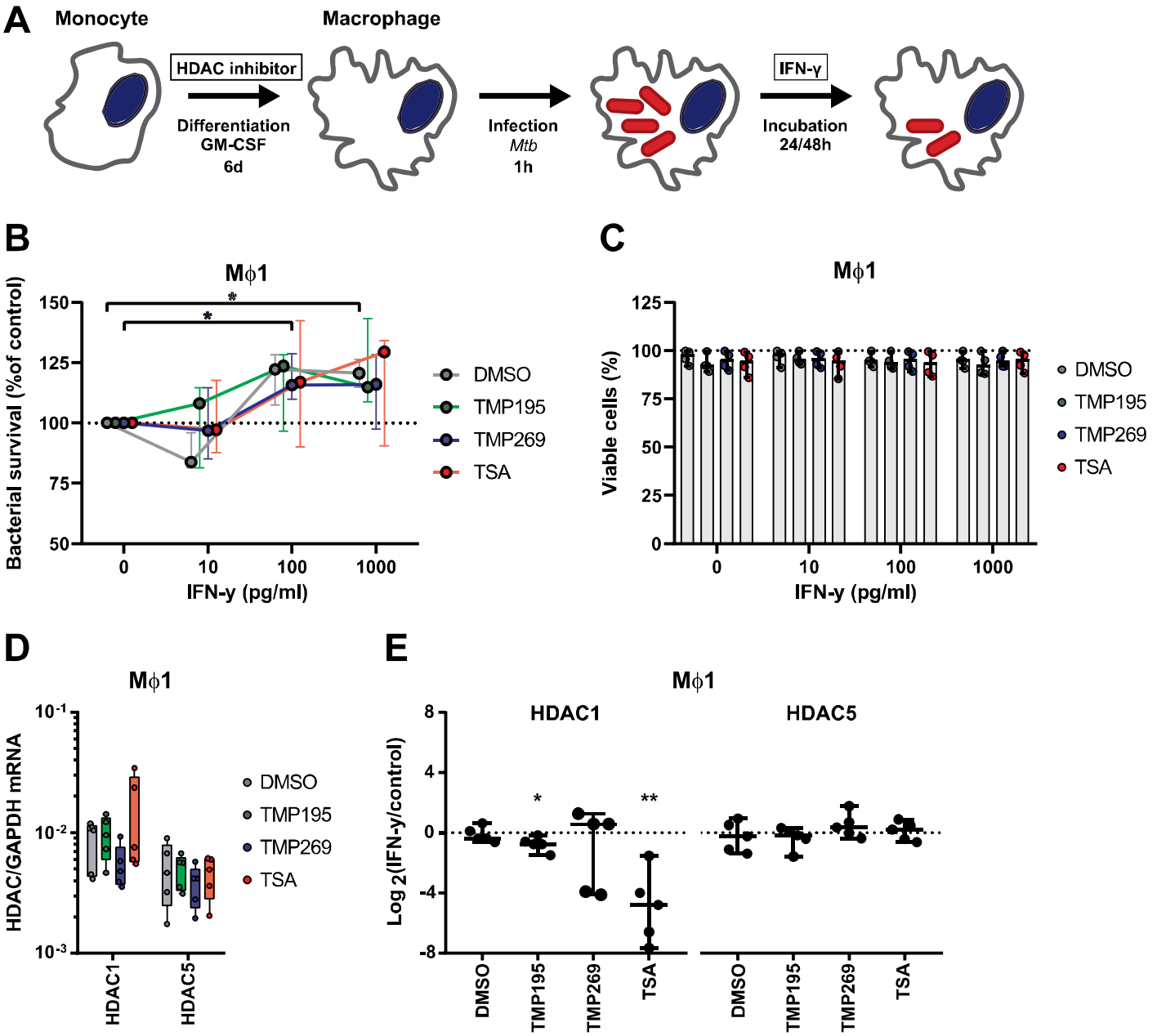
A
Monocyte
Macrophage
HDAC inhibitor
Differentiation
GM-CSF
6d
Infection
Mtb
1h
IFN-γ
Incubation
24/48h
B
Mϕ1
Bacterial survival (%of control)
150
125
100
75
50
0
10
100
1000
IFN-γ (pg/ml)
DMSO
TMP195
TMP269
TSA
C
Mϕ1
Viable cells (%)
125
100
75
50
25
0
0
10
100
1000
IFN-γ (pg/ml)
DMSO
TMP195
TMP269
TSA
D
Mϕ1
HDAC/GAPDH mRNA
10-1
10-2
10-3
HDAC1
HDAC5
DMSO
TMP195
TMP269
TSA
E
Mϕ1
HDAC1
HDAC5
Log 2(IFN-γ/control)
8
4
0
-4
-8
*
**
DMSO
TMP195
TMP269
TSA
DMSO
TMP195
TMP269
TSA

Supplementary Figure 5. Inhibition of HDAC activity during monocyte differentiation modifies the mRNa levels of some cytokine/chemokine in Mϕ1 upon Mtb infection.

A. Outline of the experimental setup used in S5B-D. B. Monocytes derived from 4 different donors were differentiated towards Mϕ1 while being exposed to TMP195 (300 nM), TMP269 (300 nM), TSA (30 nM) or DMSO at equal v/v for 6 days. Differentiated Mϕ1 were subsequently infected with *Mtb* for 1h at MOI 10 and incubated for 48 hours with different amount of IFN-γ. Dots depict the median of 4 donors, each representing the mean of 3 CFU assay replicates expressed as a percentage of the DMSO control, and whiskers represent 95% confidence intervals. Statistically significant differences compared to absence of IFN-γ were tested using a RM one-way ANOVA with repeated measures and Dunnett's multiple test correction. C. Cell viability measurement of *Mtb*-infected Mϕ1 (experimental setup as in A). Dots represent the mean of 2 viability assay replicates of a single donor expressed as a percentage of the DMSO control. Bars indicate median values of all 4 donors and whiskers represent 95% confidence intervals. Statistically significant differences compared to absence of IFN-γ were tested using a RM one-way ANOVA. D. Quantification of HDAC1 and HDAC5 transcript levels of Mϕ1, exposed to TMP195 (300 nM), TMP269 (300 nM), TSA (30 nM) or DMSO at equal v/v during differentiation, following 24 hours of *Mtb* infection. mRNA levels were determined in duplicate using qRT-PCR analysis in Mϕ1 derived from 5 different donors. Data was normalized to GAPDH ($(2^{-\Delta CT(HDAC)})/(2^{-\Delta CT(GAPDH)})$) and mean expression levels of duplicate samples were calculated for each donor. Box-and-whisker plots (min. to max.) show gene expression levels of the 5 donors where each dot represents a single donor. Significant differences between macrophage subsets were determined using a RM one-way ANOVA with Dunnett's multiple test correction. E. Quantification of HDAC1 and HDAC5 transcript levels of Mϕ1, exposed to TMP195 (300 nM), TMP269 (300 nM), TSA (30 nM) or DMSO at equal v/v during differentiation, following 24 hours of *Mtb* infection in the presence or absence of IFN-γ (1000 pg/ml). mRNA levels were determined in duplicate using qRT-PCR analysis in Mϕ1 derived from 5 different donors. Data was normalized to GAPDH and mean expression levels of duplicate samples were calculated for each donor. Dot plots display log2 FC expression levels of HDAC1 and HDAC5 to their respective baseline controls which is Mϕ1 in the absence of IFN-γ, using the formula $2^{-\Delta\Delta CT}$. Significant differences between presence and absence of IFN-γ were determined using a paired sample t-test (* = $p<0.05$, ** = $p<0.01$).

Supplementary Tables

Supplementary Table 1. Exposure to low concentrations HDAC inhibitors during monocyte differentiation alters the cytokine/chemokine response of Mϕ1 and Mϕ2 upon Mtb infection.

		Mϕ1		**Mϕ2**		**Mϕ1**				**Mϕ2**			
		Mock	*Mtb*	Mock	*Mtb*	DMSO	TMP 195	TMP 269	TSA	DMSO	TMP 195	TMP 269	TSA
Anti-inflammatory	IL-10	5	124	28	759	32	10	10	10	756	806	782	348
	IL-1ra	1890	4079	155	406	2255	1861	1303	3547	593	527	651	666
Pro-inflammatory	TNF-a	59	4548	25	778	1086	384	457	639	440	911	593	899
	IL-6	20	723	9	243	64	16	14	26	226	112	98	147
	GM-CSF	5	138	5	25	36	11	11	15	79	78	78	80
	IL-1b	3	46	3	9	4	3	3	3	35	19	21	40
	G-CSF	34	319	30	67	95	16	18	16	277	205	253	265
	IL-12p40	6	49	6	11	17	12	12	8	8	8	12	8
	IL-17a	6	12	5	14	31	23	17	20	64	57	59	43
	IFN-g	35	35	35	35	13	2	2	2	38	25	36	30
Chemokines	MIP-1a	182	2249	37	1514	1373	437	494	702	256	229	129	552
	MIP-1b	321	4707	119	2659	1000	645	502	684	548	633	491	682
	RANTES	21	180	3	40	55	35	35	35	35	35	35	35
	IP-10	35	235	33	587	3	12	3	12	74	81	100	56
	GRO	501	3332	1666	8271	430	104	277	179	3464	2559	4051	1809
	MCP-3	156	545	31	197	76	28	44	78	33	29	38	59
	IL-8	1102	8770	3316	9649	4100	1226	1372	2200	8265	8265	8265	8265
	MCP-1	4428	6938	1079	8692	2484	1331	1499	2751	2500	2058	2227	4045
	MDC	10000	10000	123	88	5806	6413	3664	4777	133	229	177	80
	EGF	33	33	33	33	4	5	5	4	28	16	22	21
	Eotaxin	8	4	6	11	16	9	16	17	41	24	44	41

Shown are median cytokine/chemokine expression levels (of 4 different donors) in supernatants of standardly differentiated Mϕ1 and Mϕ2 24h following Mtb or mock infection (first 4 columns) or in supernatants of Mϕ1 and Mϕ2 exposed to TMP195 (300 nM), TMP269 (300 nM), TSA (30 nM) or DMSO at equal v/v during differentiation (right 8 columns). Of the 41 analytes measured, only cytokines/chemokines that changed in at least 3 out of 4 donors and exhibited a minimal median log2 fold change (FC) of 0.5 in a single comparison are shown.

Supplementary Table 2. Regulation of cytokine/chemokine expression by HDACs in phagocytes

Class	HDAC enzyme	Analyte	Immunostimulatory agent	Method of interference	Cell type	Ref
I	HDAC1	IL-1β	LPS + IFN-γ	siRNA	RAW 264.7	[491]
		IL-12p40	*Mtb*	siRNA	THP-1	[455]
		IL-8	LPS	siRNA	GM-CSF differentiated human Mϕ	[492]
		IL-1β, IL-10, IL12p40, TNF-α	LPS + IFN-γ	MS-275	RAW 264.7	[493]
		IL-1β, IL-10	LPS	MS-275	RAW 264.7	[494]
		IL-6, IL-10, IL-12, TNF-α	poly(I:C)	MS-275	IL-4 + GM-CSF differentiated human DC	[495]
I	HDAC2	IL-1β, IL-1ra	LPS	Ky-2	THP-1	[496]
		MIP-2α, TNF-α	LPS	Overexpression Theophylline	RAW 264.7, PMϕ	[497]
		IL-12p70, TNF-α	LPS	shRNA	RAW 264.7, BMMϕ	[498]
		IL-6	LPS	siRNA	IL-4 + GM-CSF differentiated BMDC	[499]
I	HDAC3	IL-1β, IL-6, IL-10, IL-12p40	LPS + IFNγ	siRNA RGFP966	RAW 264.7	[491]
		IL-1β, IL-8	LPS	siRNA	GM-CSF differentiated human Mϕ	[492]
		IL-6	LPS	Scriptaid/ RGFP966	LPS differentiated BMMϕ	[500]
		IL-6, IFN-β	LPS	KO mice	BMMϕ	[501]
		TNF-α	LPS	siRNA/ overexpression	U937	[502]
IIa	HDAC4	IL-6, TNF-α	LPS	siRNA	BV2	[503]
IIa	HDAC5	IL-6, IL-10, MCP-1, TNF-α	LPS	siRNA/ overexpression	RAW 264.7	[504]
		IL-1β, IL-6, TNF-α	*Mycoplasma pneumoniae*	siRNA/ overexpression	THP-1	[505]
		IL-10, IL-12p40, IFN-γ	*Mtb*	siRNA/ overexpression	THP-1	[506]

IIb	HDAC6	IL-1β	LPS + ATP	shRNA	BMMϕ	[507]
		IL-1β, IL-6, TNF-α	Unstimulated	overexpression Tubastatin A	RAW 264.7	[508]
		IL-6, TNF-α	LPS	Tubastatin A	RAW 264.7, M-CSF differentiated BMMϕ	[451]
		IL-10	LPS	shRNA	RAW 264.7, PMϕ IL-4 + GM-CSF differentiated BMDC	[509]
		IL-10	LPS	Overexpression	RAW 264.7, THP-1, IL-4 + GM-CSF differentiated human DC	[510]
		IL-6, TNF-α	LPS	Tubastatin A	THP-1	[511]
IIa	HDAC7	IL-6, IL-12p40, TNF-α	LPS	Overexpression Compound 6a	RAW 264.7	[512]
I	HDAC8	IL-6*, IL-1β, TNF-α*	LPS	WK2-16	THP-1	[513]
IIa	HDAC9	IL-1β, IL-6, TNF-α	LPS	siRNA	RAW 264.7	[514]
IIb	HDAC10	Unknown				
IV	HDAC11	IL-10, IL-12p40, IFN-γ	*Mtb*	siRNA/ overexpression	THP-1	[506]
		IL-10	LPS	shRNA	RAW 264.7	[509]
		IL-10, IL-12p70	LPS	Overexpression	RAW 264.7, THP-1, IL-4 + GM-CSF differentiated human DC	[510]
		IL-10, IL-12p70	*Leishmania donovani*	Overexpression	RAW 264.7	[515]
		IL-10, IL-12p70	Unstimulated	siRNA/ overexpressio	THP-1, NOMO-1	[516]
		IL-10	LPS	siRNA	RAW 264.7	[517]
		IL-10, IL-12p70	LPS	siRNA	PMϕ	[518]

Positive regulation of cytokines/chemokines is shown in red, negative regulation is indicated in blue.

* Findings have been validated *in vivo* in mice.

Abbreviations: PMϕ (peritoneal elicited macrophages), BMMϕ (bone marrow-derived macrophages), BMDC (bone marrow-derived dendritic cells)

Conflict of Interest

The authors declare that the research was conducted in the absence of any commercial or financial relationships that could be construed as a potential conflict of interest.

Author Contributions

JDM, BK, SvV, MTH and KVW designed and performed the experiments and processed the experimental data. JDM, BK, MTH, FV, TMG, HPS, AHM, THMO and MCH contributed to the interpretation of the results. JDM, MTH, THMO and MCH wrote the manuscript and designed the figures with input from FV. MCH supervised the project and all authors approved the final version of the manuscript.

Funding

This project was funded by grants from the Netherlands Organization for Health Research and Development (ZonMw-TOP grant 91214038), NWO Domain Applied and Engineering Sciences (NWO-TTW grant 13259), the Brazilian Federal Agency for Support and Evaluation of Graduate Education (CAPES) and the EU-ToxRisk project (An Integrated European "Flagship" Program Driving Mechanism-Based Toxicity Testing and Risk Assessment for the 21st Century) funded by the European Commission under the Horizon 2020 program (Grant Agreement No. 681002). The funders had no role in study design, data collection and analysis, decision to publish, or preparation of the manuscript. The authors declare that they have no conflicting interests.

Acknowledgements

We gratefully acknowledge Dr J. Bestebroer (VUMC, Amsterdam, The Netherlands) for mycobacterial reporter constructs and Prof. dr. H.S. Overkleeft (Leiden Academic Centre for Drug Research, Leiden University, Leiden, The Netherlands) for synthesizing H-89 analogue 97i.

References

1. *Global tuberculosis report 2019*. 2019, Geneva, World Health Organization.
2. Becker, D., et al., Robust Salmonella metabolism limits possibilities for new antimicrobials. Nature, 2006. **440**(7082): p. 303.
3. Upadhyay, S., E. Mittal, and J.A. Philips, *Tuberculosis and the art of macrophage manipulation*. Pathog Dis, 2018. **76**(4).
4. Srivastava, S., J.D. Ernst, and L. Desvignes, *Beyond macrophages: the diversity of mononuclear cells in tuberculosis*. Immunol Rev, 2014. **262**(1): p. 179–92.
5. Benoit, M., B. Desnues, and J.-L. Mege, *Macrophage polarization in bacterial infections*. The Journal of Immunology, 2008. **181**(6): p. 3733–3739.
6. Patel, U., et al., Macrophage polarization in response to epigenetic modifiers during infection and inflammation. Drug Discov Today, 2017. **22**(1): p. 186–193.
7. Khosla, S., G. Sharma, and I. Yaseen, *Learning epigenetic regulation from mycobacteria*. Microbial Cell, 2016. **3**(2): p. 92.
8. Verdone, L., M. Caserta, and E. Di Mauro, *Role of histone acetylation in the control of gene expression*. Biochem Cell Biol, 2005. **83**(3): p. 344–53.
9. Seto, E. and M. Yoshida, *Erasers of histone acetylation: the histone deacetylase enzymes*. Cold Spring Harbor perspectives in biology, 2014. **6**(4): p. a018713.
10. Mullican, S.E., et al., Histone deacetylase 3 is an epigenomic brake in macrophage alternative activation. Genes & Development, 2011. **25**(23): p. 2480–2488.
11. Aung, H.T., et al., LPS regulates proinflammatory gene expression in macrophages by altering histone deacetylase expression. FASEB J, 2006. **20**(9): p. 1315–27.
12. Yan, B., et al., HDAC6 deacetylase activity is critical for lipopolysaccharide-induced activation of macrophages. PLoS One, 2014. **9**(10): p. e110718.
13. Shakespear, M.R., et al., Histone Deacetylase 7 Promotes Toll-like Receptor 4-dependent Proinflammatory Gene Expression in Macrophages. Journal of Biological Chemistry, 2013. **288**(35): p. 25362–25374.
14. Marino, S., et al., Macrophage polarization drives granuloma outcome during Mycobacterium tuberculosis infection. Infect Immun, 2015. **83**(1): p. 324–38.
15. Huang, L., et al., Growth of Mycobacterium tuberculosis in vivo segregates with host macrophage metabolism and ontogeny. J Exp Med, 2018. **215**(4): p. 1135–1152.
16. Wang, Y., et al., Mycobacteria inhibition of IFN-γ induced HLA-DR gene expression by up-regulating histone deacetylation at the promoter region in human THP-1 monocytic cells. The Journal of Immunology, 2005. **174**(9): p. 5687–5694.
17. Chandran, A., et al., Mycobacterium tuberculosis infection induces HDAC1-mediated suppression of IL-12B gene expression in macrophages. Frontiers in cellular and infection microbiology, 2015. **5**: p. 90.
18. Moores, R.C., et al., Epigenetic Regulation of Matrix Metalloproteinase-1 and -3 Expression in Mycobacterium tuberculosis Infection. Front Immunol, 2017. **8**: p. 602.
19. Schmeck, B., et al., Histone acetylation and flagellin are essential for Legionella pneumophila-induced cytokine expression. J Immunol, 2008. **181**(2): p. 940–7.
20. Ramakrishnan, L., *The zebrafish guide to tuberculosis immunity and treatment*. Cold Spring Harb Symp Quant Biol, 2013. **78**: p. 179–92.
21. Meijer, A.H., Protection and pathology in TB: learning from the zebrafish model. Semin Immunopathol, 2016. **38**(2): p. 261–73.
22. Cronan, M.R. and D.M. Tobin, *Fit for consumption: zebrafish as a model for tuberculosis*. Disease Models & Mechanisms, 2014. **7**(7): p. 777–784.
23. Verreck, F.A., et al., Phenotypic and functional profiling of human proinflammatory type-1 and anti-inflammatory type-2 macrophages in response to microbial antigens and IFN-gamma- and CD40L-mediated costimulation. J Leukoc Biol, 2006. **79**(2): p. 285–93.
24. Korbee, C.J., et al., Combined chemical genetics and data-driven bioinformatics approach identifies receptor tyrosine kinase inhibitors as host-directed antimicrobials. Nat Commun, 2018. **9**(1): p. 358.
25. Lobera, M., et al., Selective class IIa histone deacetylase inhibition via a nonchelating zinc-binding group. Nature chemical biology, 2013. **9**(5): p. nchembio. 1223.
26. Guerriero, J.L., et al., Class IIa HDAC inhibition reduces breast tumours and metastases through anti-tumour macrophages. Nature, 2017. **543**(7645): p. 428.

27. Roger, T., et al., Histone deacetylase inhibitors impair innate immune responses to Toll-like receptor agonists and to infection. Blood, 2011. **117**(4): p. 1205–17.
28. Takaki, K., et al., Evaluation of the pathogenesis and treatment of Mycobacterium marinum infection in zebrafish. Nat Protoc, 2013. **8**(6): p. 1114–24.
29. Benard, E.L., et al., Infection of zebrafish embryos with intracellular bacterial pathogens. J Vis Exp, 2012(61).
30. Stoop, E.J.M., et al., Zebrafish embryo screen for mycobacterial genes involved in the initiation of granuloma formation reveals a newly identified ESX-1 component. Disease Models & Mechanisms, 2011. **4**(4): p. 526–536.
31. Westergren, G. and B. Krasse, Evaluation of a micromethod for determination of Streptococcus mutans and Lactobacillus infection. J Clin Microbiol, 1978. **7**(1): p. 82–3.
32. Livak, K.J. and T.D. Schmittgen, Analysis of relative gene expression data using real-time quantitative PCR and the 2− ΔΔCT method. methods, 2001. **25**(4): p. 402–408.
33. Westerhuis, J.A., et al., *Multivariate paired data analysis: multilevel PLSDA versus OPLSDA*. Metabolomics, 2010. **6**(1): p. 119–128.
34. Rohart, F., et al., mixOmics: An R package for 'omics feature selection and multiple data integration. PLoS computational biology, 2017. **13**(11): p. e1005752.
35. KW, H. and M. AI, Time Series Modelling of Water Resources and Environmental Systems. Developments in Water Science, 1994. **45**.
36. Schindelin, J., et al., *Fiji: an open-source platform for biological-image analysis*. Nat Methods, 2012. **9**(7): p. 676–82.
37. Blischak, J.D., et al., Mycobacterial infection induces a specific human innate immune response. Scientific reports, 2015. **5**: p. 16882.
38. Roy, S., et al., Transcriptional landscape of Mycobacterium tuberculosis infection in macrophages. Scientific Reports, 2018. **8**.
39. Kuijl, C., et al., Intracellular bacterial growth is controlled by a kinase network around PKB/AKT1. Nature, 2007. **450**(7170): p. 725.
40. van der Vaart, M., et al., The DNA damage-regulated autophagy modulator DRAM1 links mycobacterial recognition via TLR-MYD88 to autophagic defence [corrected]. Cell Host Microbe, 2014. **15**(6): p. 753–67.
41. Tobin, D.M., et al., The lta4h Locus Modulates Susceptibility to Mycobacterial Infection in Zebrafish and Humans. Cell, 2010. **140**(5): p. 717–730.
42. Warga, R.M., D.A. Kane, and R.K. Ho, Fate Mapping Embryonic Blood in Zebrafish: Multi- and Unipotential Lineages Are Segregated at Gastrulation. Developmental Cell, 2009. **16**(5): p. 744–755.
43. Ottenhoff, T.H.M., et al., Genetics, cytokines and human infectious disease: lessons from weakly pathogenic mycobacteria and salmonellae. Nature Genetics, 2002. **32**(1): p. 97–105.
44. Etna, M.P., et al., Pro- and anti-inflammatory cytokines in tuberculosis: a two-edged sword in TB pathogenesis. Semin Immunol, 2014. **26**(6): p. 543–51.
45. Seshadri, C., et al., Transcriptional networks are associated with resistance to Mycobacterium tuberculosis infection. PLoS One, 2017. **12**(4): p. e0175844.
46. Simmons, J.D., et al., Immunological mechanisms of human resistance to persistent Mycobacterium tuberculosis infection. Nat Rev Immunol, 2018. **18**(9): p. 575–589.
47. Wang, X., et al., Histone deacetylase 6 inhibitor enhances resistance to Mycobacterium tuberculosis infection through innate and adaptive immunity in mice. Pathog Dis, 2018. **76**(6).
48. Trede, N.S., et al., *The use of zebrafish to understand immunity.* Immunity, 2004. **20**(4): p. 367–379.
49. Davis, J.M., et al., Real-time visualization of Mycobacterium-macrophage interactions leading to initiation of granuloma formation in zebrafish embryos. Immunity, 2002. **17**(6): p. 693–702.
50. Lee, H.J., et al., Lysophosphatidylcholine Promotes Phagosome Maturation and Regulates Inflammatory Mediator Production Through the Protein Kinase A-Phosphatidylinositol 3 Kinase-p38 Mitogen-Activated Protein Kinase Signalling Pathway During Mycobacterium tuberculosis Infection in Mouse Macrophages. Front Immunol, 2018. **9**: p. 920.
51. Mendez-Samperio, P., A. Trejo, and E. Miranda, Activation of ERK1/2 and TNF-alpha production are mediated by calcium/calmodulin, and PKA signalling pathways during Mycobacterium bovis infection. J Infect, 2006. **52**(2): p. 147–53.
52. Walkinshaw, D.R., et al., Dephosphorylation at a conserved SP motif governs cAMP sensitivity and nuclear localization of class IIa histone deacetylases. Journal of Biological Chemistry, 2013. **288**(8): p. 5591–5605.
53. Liu, Y. and M.F. Schneider, Opposing HDAC4 nuclear fluxes due to phosphorylation by beta-adrenergic activated protein kinase A or by activity or Epac activated CaMKII in skeletal muscle fibres. J Physiol, 2013. **591**(14): p. 3605–23.
54. Zhu, C.Z., et al., Histone deacetylase inhibitors impair the host immune response against Mycobacterium tuberculosis infection. Tuberculosis, 2019. **118**.

55. Coussens, A.K., R.J. Wilkinson, and A.R. Martineau, Phenylbutyrate Is Bacteriostatic against Mycobacterium tuberculosis and Regulates the Macrophage Response to Infection, Synergistically with 25-Hydroxy-Vitamin D-3. Plos Pathogens, 2015. **11**(7).
56. Domingo-Gonzalez, R., et al., *Cytokines and chemokines in Mycobacterium tuberculosis infection.* Microbiology spectrum, 2016. **4**(5).
57. Cui, S.N., et al., Trichostatin A modulates the macrophage phenotype by enhancing autophagy to reduce inflammation during polymicrobial sepsis. Int Immunopharmacol, 2019: p. 105973.
58. Songane, M., et al., The role of autophagy in host defence against Mycobacterium tuberculosis infection. Tuberculosis (Edinb), 2012. **92**(5): p. 388–96.
59. Clocchiatti, A., et al., Class IIa HDACs repressive activities on MEF2-depedent transcription are associated with poor prognosis of ER(+) breast tumors. FASEB J, 2013. **27**(3): p. 942–54.
60. Koenis, D.S., et al., Nuclear Receptor Nur77 Limits the Macrophage Inflammatory Response through Transcriptional Reprogramming of Mitochondrial Metabolism. Cell Rep, 2018. **24**(8): p. 2127–2140 e7.
61. Hamers, A.A., et al., Bone marrow-specific deficiency of nuclear receptor Nur77 enhances atherosclerosis. Circ Res, 2012. **110**(3): p. 428–38.
62. Hanna, R.N., et al., NR4A1 (Nur77) deletion polarizes macrophages toward an inflammatory phenotype and increases atherosclerosis. Circ Res, 2012. **110**(3): p. 416–27.
63. Gregoire, S., et al., Control of MEF2 transcriptional activity by coordinated phosphorylation and sumoylation. J Biol Chem, 2006. **281**(7): p. 4423–33.
64. Gregoire, S. and X.J. Yang, Association with class IIa histone deacetylases upregulates the sumoylation of MEF2 transcription factors. Mol Cell Biol, 2005. **25**(6): p. 2273–87.
65. Leus, N.G., et al., HDAC 3-selective inhibitor RGFP966 demonstrates anti-inflammatory properties in RAW 264.7 macrophages and mouse precision-cut lung slices by attenuating NF-kappaB p65 transcriptional activity. Biochem Pharmacol, 2016. **108**: p. 58–74.
66. Winkler, A.R., K.N. Nocka, and C.M. Williams, Smoke exposure of human macrophages reduces HDAC3 activity, resulting in enhanced inflammatory cytokine production. Pulm Pharmacol Ther, 2012. **25**(4): p. 286–92.
67. Leus, N.G., et al., HDAC1-3 inhibitor MS-275 enhances IL10 expression in RAW264.7 macrophages and reduces cigarette smoke-induced airway inflammation in mice. Sci Rep, 2017. **7**: p. 45047.
68. Zhang, Z.Y. and H.J. Schluesener, HDAC inhibitor MS-275 attenuates the inflammatory reaction in rat experimental autoimmune prostatitis. Prostate, 2012. **72**(1): p. 90–9.
69. Nencioni, A., et al., Histone deacetylase inhibitors affect dendritic cell differentiation and immunogenicity. Clinical Cancer Research, 2007. **13**(13): p. 3933–3941.
70. Kaneko, J., et al., Ky-2, a hybrid compound histone deacetylase inhibitor, regulated inflammatory response in LPS-driven human macrophages. Cell Biol Int, 2018. **42**(12): p. 1622–1631.
71. Fang, W.F., et al., Histone deacetylase 2 (HDAC2) attenuates lipopolysaccharide (LPS)-induced inflammation by regulating PAI-1 expression. J Inflamm (Lond), 2018. **15**: p. 3.
72. Wu, C., et al., Histone deacetylase 2 is essential for LPS-induced inflammatory responses in macrophages. Immunol Cell Biol, 2018.
73. Zhang, Q., et al., Tet2 is required to resolve inflammation by recruiting Hdac2 to specifically repress IL-6. Nature, 2015. **525**(7569): p. 389–393.
74. Sanchez, S., et al., HDAC3 Inhibition Promotes Alternative Activation of Macrophages but Does Not Affect Functional Recovery after Spinal Cord Injury. Exp Neurobiol, 2018. **27**(5): p. 437–452.
75. Chen, X., et al., Requirement for the histone deacetylase Hdac3 for the inflammatory gene expression program in macrophages. Proc Natl Acad Sci U S A, 2012. **109**(42): p. E2865–74.
76. Mahlknecht, U., et al., Histone deacetylase 3, a class I histone deacetylase, suppresses MAPK11-mediated activating transcription factor-2 activation and represses TNF gene expression. J Immunol, 2004. **173**(6): p. 3979–90.
77. Wang, B., et al., Glycolysis-dependent histone deacetylase 4 degradation regulates inflammatory cytokine production. Molecular biology of the cell, 2014. **25**(21): p. 3300–3307.
78. Poralla, L., et al., *Histone deacetylase 5 regulates the inflammatory response of macrophages.* Journal of cellular and molecular medicine, 2015. **19**(9): p. 2162–2171.
79. Zhao, Y., G. Ma, and X. Yang, HDAC5 promotes Mycoplasma pneumoniae-induced inflammation in macrophages through NF-kappaB activation. Life Sci, 2019. **221**: p. 13–19.
80. Wang, X., et al., Mycobacterium tuberculosis infection induces IL-10 gene expression by disturbing histone deacetylase 6 and histonedeacetylase 11 equilibrium in macrophages. Tuberculosis (Edinb), 2018. **108**: p. 118–123.
81. Hwang, I., et al., *Histone deacetylase 6 negatively regulates NLRP3 inflammasome activation.* Biochem Biophys Res Commun, 2015. **467**(4): p. 973–8.

82. Youn, G.S., et al., Overexpression of HDAC6 induces pro-inflammatory responses by regulating ROS-MAPK-NF-kappaB/AP-1 signalling pathways in macrophages. Free Radic Biol Med, 2016. **97**: p. 14–23.
83. Cheng, F., et al., Divergent roles of histone deacetylase 6 (HDAC6) and histone deacetylase 11 (HDAC11) on the transcriptional regulation of IL10 in antigen presenting cells. Mol Immunol, 2014. **60**(1): p. 44–53.
84. Villagra, A., et al., The histone deacetylase HDAC11 regulates the expression of interleukin 10 and immune tolerance. Nat Immunol, 2009. **10**(1): p. 92–100.
85. Vishwakarma, S., et al., Tubastatin, a selective histone deacetylase 6 inhibitor shows anti-inflammatory and anti-rheumatic effects. Int Immunopharmacol, 2013. **16**(1): p. 72–8.
86. Shakespear, M.R., et al., Histone deacetylase 7 promotes Toll-like receptor 4-dependent proinflammatory gene expression in macrophages. J Biol Chem, 2013. **288**(35): p. 25362–74.
87. Jan, J.S., et al., The Novel HDAC8 Inhibitor WK2-16 Attenuates Lipopolysaccharide-Activated Matrix Metalloproteinase-9 Expression in Human Monocytic Cells and Improves Hypercytokinemia In Vivo. Int J Mol Sci, 2017. **18**(7).
88. Pham, T.X., et al., Transcriptional and posttranscriptional repression of histone deacetylases by docosahexaenoic acid in macrophages. J Nutr Biochem, 2018. **57**: p. 162–169.
89. Mukherjee, S., et al., Imipramine exploits histone deacetylase 11 to increase the IL-12/IL-10 ratio in macrophages infected with antimony-resistant Leishmania donovani and clears organ parasites in experimental infection. J Immunol, 2014. **193**(8): p. 4083–94.
90. Shinohara, H., et al., Regulated Polarization of Tumor-Associated Macrophages by miR-145 via Colorectal Cancer-Derived Extracellular Vesicles. J Immunol, 2017. **199**(4): p. 1505–1515.
91. Bala, S., et al., Alcohol-induced miR-155 and HDAC11 inhibit negative regulators of the TLR4 pathway and lead to increased LPS responsiveness of Kupffer cells in alcoholic liver disease. J Leukoc Biol, 2017. **102**(2): p. 487–498.
92. Lin, L., et al., Type I IFN inhibits innate IL-10 production in macrophages through histone deacetylase 11 by downregulating microRNA-145. J Immunol, 2013. **191**(7): p. 3896–904.